ATOMIC LAYER THERMOPILE FILM FOR HEAT FLUX MEASURMENT IN HIGH SPEED AND HIGH TEMPERATURE FLOWS

by

Lakshya Bhatnagar

A Thesis

Submitted to the Faculty of Purdue University

In Partial Fulfillment of the Requirements for the degree of

Master of Science in Mechanical Engineering

School of Mechanical Engineering

West Lafayette, Indiana

December 2018

THE PURDUE UNIVERSITY GRADUATE SCHOOL
STATEMENT OF COMMITTEE APPROVAL

Dr. Guillermo Paniagua

Department of Mechanical Engineering

Dr. Sally Bane

Department of Aeronautics and Astronautics

Dr. Amy Marconnet

Department of Mechanical Engineering

Approved by:

Dr. Jay P Gore

Head of the Graduate Program

ACKNOWLEDGMENTS

The author will like to thank Dr. J Betz for his help on the technical details of the ALTP and his timely repair of the damaged sensor. The author will also like to thank J Saavedra and J Braun for allowing to test in their respective test articles. The author will like to recognize Dr. Guillermo Paniagua, Dr. Sally Bane and Dr. Amy Marconnet for their support and guidance throughout this project.

TABLE OF CONTENTS

LIST OF TABLES 6
LIST OF FIGURES 7
ABSTRACT 12
CHAPTER 1. OBJECTIVE AND METHODOLOGY 13
1.1 Objectives 13
1.2 Methodology 13
1.2.1 Development of precise calibration methodology for accurate uncertainty estimation. 14
1.2.2 Experiments in High Speed Shock Wave environment. 14
1.2.3 Design of cooling system for measurement in hot conditions inside combustor 15
CHAPTER 2. DEVELOPMENT OF UNCERTAINTY QUANTIFICATION TOOLS 16
2.1 Review of Atomic Layer Thermopile and principle of Operation 16
2.1.1 Theory and Model of the Atomic Layer Thermopile 16
2.1.2 Adaptation of the ALTP as a Sensor 19
2.2 Review of Heat Flux Calibration Techniques using Atomic Layer Thermopile film 22
2.2.1 Static Calibration through exposure to Radiation 22
2.2.2 Dynamic Calibration through laser exposure 24
2.2.3 Calibration of Heat Flux Sensors in a Convective Environment 24
2.2.4 Heat Flux Measurement in Turbomachinery 25
2.3 Calibration Through exposure to radiation 27
2.3.1 Description of Experimental Setup 27
2.3.2 Uncertainty Estimation 30
2.3.3 Results 30
2.4 Calibration by Electrical Measurement 34
2.4.1 Description of Experimental Setup 34
2.4.2 Uncertainty Estimation 37
2.4.3 Results 40
2.4.4 Limitations 41
2.5 Calibration using Heat Flux calculated by Transient Convective Heat Transfer 41

2.5.1 Description of Experimental Setup 41
2.5.2 Thermocouple Calibration 47
2.5.3 Uncertainty Estimation 50
2.5.4 Results 52
2.5.5 Limitations 57
CHAPTER 3. HEAT FLUX MEASUREMENT IN HIGH SPEED SHOCK WAVE ENVIRONMENT 59
3.1 Review 59
3.2 Experimental Methodology and test conditions 60
3.3 Experimental Uncertainty 62
3.4 Results and Discussion 63
CHAPTER 4. DESIGN OF COOLING SYSTEM FOR COMBUSTOR HEAT FLUX MEASUREMENT 68
4.1 Review of Heat Flux measurement in combustors 68
4.2 Review of cooling strategies applied to probes for high temperature 68
4.3 Description of the ALTP cooling problem 69
4.4 1D Model 71
4.4.1 Model Description 71
4.4.2 Limitations 74
4.5 2D axisymmetric numerical simulation 75
4.5.1 Geometry Description 75
4.5.2 Boundary Conditions 76
4.5.3 Mesh Sensitivity 77
4.5.4 CFD Results and Discussion 79
4.6 2D axisymmetric Structural Analysis 83
4.6.1 Geometry Description 83
4.6.2 Boundary Conditions 83
4.6.3 Mesh Description 84
4.6.4 Results and Discussion 85
CHAPTER 5. CONCLUSIONS 88
REFERENCES 78

LIST OF TABLES

Table 2.1 Pre Experiment Uncertainty Estimation 39

Table 2.2 Uncertainty table for heat flux value based on the Kapton and Aluminium layer 51

Table 2.3 Uncertainty table for heat flux based on the ALTP film and substrate system 52

LIST OF FIGURES

Figure 2.1 Plane Thermopile generated by two material of different Seebeck coeffieint S_A and S_B [10]. 16

Figure 2.2 Unit cell structure of $YBa_2Cu_3O_{7-\delta}$ [15]. 17

Figure 2.3 Schematic of a ALTP film on a SrTio3 substrate, d is the thickness of the film, n is the surface normal, α is the angle between the surface normal and the c axis of the crystal [16]. 18

Figure 2.4 Schematic of the ALTP sensor with the electrical connections and thermocouple position [16]. 20

Figure 2.5 Photos of the ALTP probe, a)Top view of the ALTP Probe with the film position highlighted, b) Front view of the ALTP probe showing the different layers of the probe body, c) Schematic of the inner cut section of the ALTP probe. 21

Figure 2.6 Typical Laser calbration setup for static calibration of ALTP [16]. 22

Figure 2.7 Test results for ALTP film showing linear nature over broad range of heat flux [16]. 23

Figure 2.8 Typical Setup for dynamic calibration of ALTP [22]. 24

Figure 2.9 The NIST convective heat flux calibration test plate [24]. 25

Figure 2.10 Schematic of Experimental Setup for calibration through exposure to radiation, the schematic shows the position of the mechanical shutter, CW laser and the location of the sensor holder and the power meter with respect to each other 29

Figure 2.11 CCD image showing laser beam spot and pixels which were used to estimate the beam diameter. 29

Figure 2.12 ALTP signal output at given laser power. 31

Figure 2.13 Calibration curves showing linearity between voltage and input heat flux for two ALTP sensors. a) ALTP sensor 1 has higher sensitivity but a slower response upto 100KHz. b) ALTP sensor 2 has lower sensitivity and lower damage threshold but a higher frequency response upto 1MHz. 32

Figure 2.14 Relative uncertainty with heat flux based on slope and intercept uncertainty. 33

Figure 2.15 Power Spectral Density spectrogram of the ALTP signal when exposed to laser burst. Each jump in PSD is an indication of either the shutter opening or closing. 33

Figure 2.16 Layout of test article. a) Assembly of copper test plate with the foil heaters and the position of the RTD's b) Assembly of the backing phenolic sheet showing the location of foil heaters and RTD. c) Back view of the backing phenolic sheet showing the location of the ALTP probe. 35

Figure 2.17 a) Layout of the test section showing the arrangement of the blower and location of the test article. b) The inner schematic of the duct. 36

Figure 2.18 Arrangement of the Fluke constant temperature well and the RTD's during calibration. 37

Figure 2.19 Calibration curve of the RTD's showing sensor resistance with well temperature. ..38

Figure 2.20 Results of the calibration showing the ALTP voltage signal with input power in terms of heater input voltage. 40

Figure 2.21 The trend of the empirically calculated heat flux based on flow parameters wall temperature for purely laminar and turbulent flow in relation to the heat flux input to the heater. 41

Figure 2.22 a) The linear wind tunnel test section at PETAl b) Opened linear test section showing the location of mounting of instrumentation. c) Location of the cabinets containing all conditioning system with respect to the wind tunnel. d) Layout of the linear wind tunnel. 43

Figure 2.23 a) Flow exposed side of the instrumentation insert showing the location of the ALTP probe and surface thermocouples. b) Outside surface of the instrumentation insert showing the location of the rear surface thermocouples, the ALTP and the thermocouple for the substrate temperature. 44

Figure 2.24 Graphical representation of the one-dimensional heat transfer code used for heat flux evaluation using thermocouples. 45

Figure 2.25 a)Schematic of the 1d heat transfer actually measured using surface thermocouples, b)Schematic of the heat transfer through the ALTP sensor. 46

Figure 2.26 Arrangement of the Fluke Temperature Well and thermocouples during calibration. 47

Figure 2.27 Calibration curve for one thermocouple showing linear trend between sensor voltage and temperature of the well. 48

Figure 2.28 Relative Uncertainty in temperature plots for different thermocouples as a function of temperature. 50

Figure 2.29 a)Temperature variation inside the test section on the opening of the valve, b)ALTP raw signal on the opening of the valve. 54

Figure 2.30 Calibration curve showing linear behavior between ALTP voltage and Heat Flux. The uncertainty bands are based on the uncertainty in prediction of Heat flux from the thermocouples. 55

Figure 2.31 Calibration Curve showing the error bands based on 95% confidence prediction interval based on statistical inferences. 56

Figure 2.32 Relative Uncertainty for heat flux for ALTP calibration based on slope and intercept uncertainty. 57

Figure 3.1 a)Supersonic flow test nozzle b)Flow exposed surface of test insert used for ALTP c)Numerical Mach contours of the nozzle showing the Mach number at the ALTP location. 61

Figure 3.2 Piping Diagram showing the piping under vacuum for supersonic flow. 61

Figure 3.3 Temperature and Pressure behavior inside the test section during one run with the supersonic nozzle with hot flow. 63

Figure 3.4 The first column shows ALTP heat flux reading for different test runs and column two shows the surface thermocouple derived heat flux. 65

Figure 3.5 ALTP signal for Run1 Hot flow at 4Hz to show sharp changes in heat flux during shock and expansion wave inside wind tunnel. 66

Figure 3.6 Decrease of heat flux with increasing wall temperature for constant flow temperature. 66

Figure 4.1 Basic schematic Geometry of the ALTP cooling system. 70

Figure 4.2 Block Diagram of the 1D model. 72

Figure 4.3 Contours of the quantities of interest from the 1D code, the water at temperature sensor , the outlet water temperature, the probe wall temperature and the mass flow rate as a function of the velocity and the parameterized radius. 74

Figure 4.4 Schematic of the basic geometry used for 2D axisymmetric study. 75

Figure 4.5 Mesh used for the 2D axisymmetric analysis with zoom in of the inflation layer and the conjugate solid-fluid interface.....78

Figure 4.6 Mesh sensitivity results for the quantities of interest, a)The behavior of the Maximum substrate temperature with number of nodes, b)the trend of the Maximum turbulent intensity of the flow with number of nodes, c)The maximum coolant temperature with number of nodes, d) The extrapolated relative error for the maximum substrate temperature based on Celik[38] definition.....78

Figure 4.7 Temperature contour of substrate a) with PGS and showing the relative distribution of heat, b) without PGS and showing the relative distribution of heat.....79

Figure 4.8 a) Geometry of the substrate analysis, b) Temperature contour of the substrate at 243K isothermal wall, c)Temperature of the substrate at 233K isothermal wall.....80

Figure 4.9 Revised geometry for 2D analysis using Magnesium Oxide and trip geometry. 81

Figure 4.10 Revised Geometry with curved channel to further enhance heat transfer by preventing separation near the wall.....82

Figure 4.11 a) Temperature contour of the coolant showing the maximum temperature below the boiling point of the coolant, b) Temperature contour of the entire system showing the peak temperature on the outer wall and the zoom in of the substrate temperature contour. 82

Figure 4.12 Basic Geometry and Boundary Conditions for the structural analysis. 83

Figure 4.13 Mesh for the 2d Structural analysis showing mesh concentration near the joints. 84

Figure 4.14 Results of the 2d structural analysis with only the pressure and shear applied, a)the radial displacement of the probe, b) the axial displacement of the probe, c) the Von-mises stress concentration of the probe. 85

Figure 4.15 Results of the 2d structural analysis with temperature conditions applied a)the radial displacement of the probe, b) the axial displacement of the probe, c) the Von-mises stress concentration of the probe. 87

ABSTRACT

Author: Bhatnagar, Lakshya, MSME
Institution: Purdue University
Degree Received: December 2018
Title: Atomic Layer Thermopile Film for Heat Flux Measurement in High Speed and High Temperature Flows
Major Professor: Guillermo Paniagua

This work seeks to apply the novel heat flux sensor called as the Atomic Layer Thermopile to measure high frequency heat flux in high speed and high temperature flows found in Gas Turbine combustors. To achieve this the sensor must be able to survive the harsh environment of high temperature and high pressure. To have any confidence in our measurement, it is also imperative that there are tools available for precise estimation of the measurement uncertainty. This works strives to achieve these objectives by developing calibration techniques for uncertainty estimation using both exposure to radiation and in convective environments by calibrating against power input in steady state flow and transient heat flux calculated using wall temperature measurement. The response of the sensor is then investigated in high speed flows by measuring the heat flux inside a supersonic nozzle when exposed to shock waves. The shock waves are generated using a fast throttle valve located at the entrance of the supersonic nozzle by generating sudden rise in pressure. Lastly a numerical study is carried out to design a cooling system that will allow the sensor to survive in high temperature conditions of 1000°C while the sensor film is maintained at 50°C. A one-dimensional model is used to provide initial design parameters and then a two-dimensional axisymmetric conjugate CFD analysis is carried out to obtain the desired geometry that can meet the design conditions. A static structural analysis is also carried out on this geometry to ensure that it will be able to survive and avoid distortion under the operational pressure required for providing the desired coolant mass flow.

CHAPTER 1. OBJECTIVE AND METHODOLOGY

1.1 Objectives

This work aims to provide a technique with which high frequency heat flux measurement data can be measured in systems with high operational temperatures and high speed flows with quantifiable and accurate uncertainty estimates. To achieve this a novel type of sensor called the atomic layer thermopile will be used. This sensor, commonly called as ALTP, has the response time in the orders of microseconds and can hence go up to 100KHz. The ALTP has been shown to have linear behavior with heat flux over several orders of magnitude, much higher than the typical values that will be seen in the scope of this work. The sensitivity of the sensor is however low and the output voltage is in terms of microvolts. This implies that the sensor is highly sensitive to uncertainties in its calibration procedure and though it has very fast response time, precise knowledge of uncertainties should be available to ensure the accuracy of the measurement.

Hence the objective of this work is three fold as listed in the following.

1. Development of technique for high frequency heat flux measurement inside a combustor
2. Implementation of ALTP for measurement of heat flux fluctuations in supersonic flow
3. Development of tools for precise uncertainty quantification of heat flux measurement

1.2 Methodology

A combination of experimental and computational methods is selected to achieve the objective of this work. Firstly, to have confidence in the measurement technique, the estimation of uncertainty is important, hence the development of uncertainty tools through experimental methods was investigated. Then the heat flux measurement technique was applied to high speed flow by ensuring its survivability in supersonic environment with shock waves. Lastly it was investigated how to apply the sensor to high temperature environments for long exposure test.

1.2.1 Development of precise calibration methodology for accurate uncertainty estimation.

To achieve precise estimates of uncertainty in the heat flux being measured, the ALTP sensor must be calibrated against a measurement of heat flux that is highly precise. Heat flux measurement is a tricky subject and most techniques suffer from high values of uncertainty. The most commonly used technique involves exposure to radiation of known power. The sensor was run through three different experimental calibrations and their results were compared to see which one should be used to achieve the objectives of this work. The exposure to radiation was investigated along with convective heat flux measurement using electrical power for steady state conditions and calibration against heat flux calculated for sudden discharge flows using wall temperature readings. It was found that the laser calibration technique has the fundamental problem of the inaccuracy in estimation of surface properties and for the setup used, very high uncertainties. The calibration through electrical measurement provided inconclusive trends and suffered greatly from the limitations of the assumption of the steady state system and uniform temperature distribution in the test article. The calibration against heat flux calculated from wall temperature readings, though an established technique in the field of turbomachinery, has its own challenges especially on the assumption of one-dimensional heat flow and different frequency response of the sensors used. The details of each methodology will be investigated in the subsequent chapters.

1.2.2 Experiments in High Speed Shock Wave environment.

The ALTP boasts a frequency response of the order of 100Khz to a 1Mhz, depending on the size of the active area. At this frequency resolution, it is an ideal sensor to pick up changes in the wall heat flux in a supersonic environment. To achieve this, the sensor was placed at the end of a supersonic nozzle and the shock waves were generated by the opening of the fast actuation valve of the wind tunnel in which it was tested. The opening of the valve generates a pressure wave, but when coupled with a supersonic nozzle, the pressure wave is converted to a supersonic shock wave. The response of the ALTP was compared against another technique used for heat flux measurement, namely calculation based on wall temperature measurements. Thin surface thermocouples were employed to measure the temperature of the surface where the ALTP was mounted to provide accurate wall temperature readings. The sensor was exposed to both cold and hot flow and it was able to pick up sharp heat flux variation as the shock wave hits the measurement

location and it is also able to measure rapid changes in heat flux which occur during flow separation when the flow regime changes from supersonic to subsonic.

1.2.3 Design of cooling system for measurement in hot conditions inside combustor

To apply the ALTP inside a high temperature environment like combustors, it need to be able to survive the high temperature environment. So a cooling system need to be developed to ensure that the ALTP film never exceeds its design conditions, which for the available sensors is 323K. A one-dimensional model was developed to provide the starting value of the design of the cooling system by breaking the system into separate blocks and solving for the average temperatures inside each block. Based on the starting value obtained from the one-dimensional code, a steady state two-dimensional axisymmetric conjugate analysis was carried out using Ansys Fluent, where the geometry of the cooling channels was optimized to achieve the design temperature. With the optimized geometry available, a two-dimensional static structural analysis was carried out to ensure the probe survivability under the operational pressure required to provide sufficient mass flow to the coolant to achieve the design temperature.

CHAPTER 2. DEVELOPMENT OF UNCERTAINTY QUANTIFICATION TOOLS

2.1 Review of Atomic Layer Thermopile and principle of Operation

2.1.1 Theory and Model of the Atomic Layer Thermopile

An Atomic Layer thermopile is the name that was given to a class of epitaxial conducting films where it was observed that a measurable voltage is generated when the surface is heated. The term was coined in the work of Lengfellner [10] which was the first time the effect of induced voltage when a film of Yttrium Barium Cupric Oxide, ($YBa_2Cu_3O_{7-\delta}$) also called as YBCO-Cu_2O, is exposed to pulsed laser and continuous heating using heaters was documented. The thermoelectric power of $YBa_2Cu_3O_{7-\delta}$ has been studied before especially for cold temperatures. Cohn's [11] work reported the measurement of the a-b plane Seebeck coefficient of the film for below 310 K and Crommie [12] discussed the anisotropic nature of that Seebeck coefficient and the thermal conductivity of $YBa_2Cu_3O_{7-\delta}$ films. Cohn[11] showed the contribution of diffusion and phonon drag on the Seebeck coefficient and was able to calculate the Seebeck coefficient for different temperatures. However, the predicted value of voltage based on this value of coefficient for small temperature differences was inconsistent with Lengfellenr's [10] observation when the film was exposed to a pulsing laser source. The explanation for this discrepancy was that the high conductivity layer in the $YBa_2Cu_3O_{7-\delta}$ layer naturally forms a series of connections like in a thermopile and this leads to the enhancement of the voltage much higher than can be achieved based on the single crystal Seebeck Coefficient.

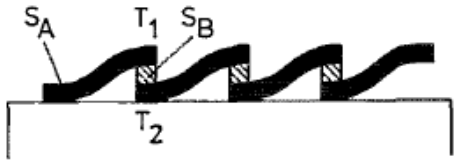

Figure 2.1 Plane Thermopile generated by two material of different Seebeck coeffieint S_A and S_B [10].

A thermopile voltage can be defined mathematically as

$$U = n(S_A - S_B)\Delta T \tag{2.1}$$

Where, n is the number of contacts, U is the induced voltage, SA and SB are the different Seebeck Coefficients of the different materials and ΔT is the temperature difference across the sensing element. For $YBa_2Cu_3O_{7-\delta}$ films it is reported [13] that there is always a small angle between the surface normal and the c-axis of the crystal and are present due to several reasons not limited to the limitations of deposit process and inconsistencies in the substrate material cutting. For the $YBa_2Cu_3O_{7-\delta}$ film the crystal structure is a repeated lattice of Yttrium and Barium layers separated between by Copper (II) Oxide in between. The Copper (II) Oxide is a lattice arrangement of coper-oxygen planes and copper-oxygen chains. Along the c axis the stacking sequence for the crystal goes as CuO-BaO-Cu2O-Y-CuO2-BaO [14]. The YBCO layers are arranged in a perovskite structure and are separated by planes of Cu_2O. The cell structure is shown in Figure 2.2

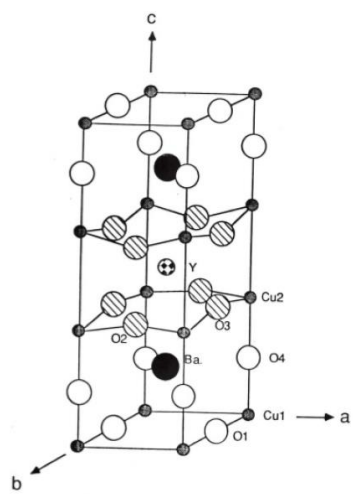

Figure 2.2 Unit cell structure of $YBa_2Cu_3O_{7-\delta}$ [15].

Based on this unit cell structure of $YBa_2Cu_3O_{7-\delta}$, Lengfellner argued that the two different arrangement of atoms in the unit cell, the YBCO layer passing through the centre of the unit cell and the Cu_2O layer on the edges of the unit cell can be treated as layers of two different material. These two layers have different Seebeck coefficient, the YBCO layer has much lower thermal conductivity than the Cu_2O layer. Hence, this structure can be treated as a thermocouple junction

on an atomic scale. These layers are generally not aligned with the normal to the surface giving the most common arrangement of the Atomic Layer thermopile film as shown in Figure 2.3.

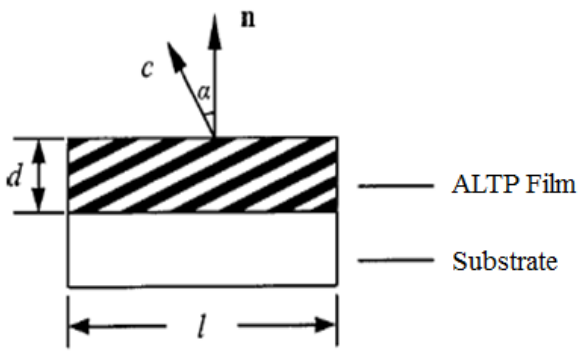

Figure 2.3 Schematic of a ALTP film on a SrTio3 substrate, d is the thickness of the film, n is the surface normal, α is the angle between the surface normal and the c axis of the crystal [16].

Based on this explanation of the ALTP film a mathematical model of the induced voltage can be made. Assuming a film thickness of d, with a temperature gradient in the vertical axis and a heat exposed length of l, based on the coordinate system of Figure 2.3, in vector terms we can write the Electric Field as in Equation (2.2)

$$\vec{E} = \vec{S}\nabla\vec{T} \tag{2.2}$$

Writing the elements of the Seebeck tensor we obtain

$$\vec{S} = \begin{bmatrix} S_{ab}\cos^2\alpha_c + S_c\sin^2\alpha_c & 0 & \frac{sin2\alpha_c}{2}(S_{ab} - S_c) \\ 0 & S_{ab} & 0 \\ \frac{(sin2\alpha_c)}{2}(S_{ab} - S_c) & 0 & S_{ab}\sin^2\alpha_c + S_c\cos^2\alpha_c \end{bmatrix} [16] \tag{2.3}$$

For a temperature difference in the y direction, the x component of voltage yields to the relation

$$V_x = \frac{E}{d} = -\varepsilon_x l = \frac{l(S_{ab} - S_c)\Delta T sin2\alpha_c}{2d} \tag{2.4}$$

This is electric voltage that is measured in a sensor that makes use of the ALTP film. Typical values of α for the ALTP is around 20° and the thickness of the film varies from sensor to sensor.

Zhang [17] in his work utilized the Carslaw and Jeager solution of the temperature distribution inside a thin film when its exposed to a point instantaneous source of heat flux to calculate dependency of the electric voltage generated by the film to the temperature distribution inside the

film. This approximation of a point instantaneous heat source is mimicked in real life conditions by sudden exposure of the film to a laser source. According to Carslaw and Jeager[18] for a material whose thickness is much small compared to its thickness exposed to a point source of heat flux at t=0, the time dependent temperature distribution in the depth of the material is given by

$$T(z,t) = \frac{Q}{\rho c_o \sqrt{4\pi D t}} e^{-\frac{z^2}{4Dt}} \tag{2.5}$$

Where T is the time dependent temperature at position z inside the material, Q is the total heat flux at t=0, ρ is the material density, c_o is the specific heat capacity and D is the diffusivity of the material. As t approaches zero, Equation (2.5) approaches infinity, hence Zhang [17] proposed to take the temperature at δ below the surface to give

$$T_1(t) = \frac{Q}{\rho c_o \sqrt{4\pi D t}} e^{-\frac{\delta^2}{4Dt}} \tag{2.6}$$

Substituting the definition of temperature in Equation (2.4) we end up with the time dependent voltage generation as a function of the material properties.

$$V_x(t) = \frac{Ql(S_{ab} - S_c)\Delta T sin2\alpha_c}{4d\rho c_o}\left(e^{-\frac{\delta^2}{4Dt}} - e^{-\frac{d^2}{4Dt}}\right) \tag{2.7}$$

This equation is though only valid for t< 2μs since then the heat transfer effect of the film and substrate and the film and surrounding become dominant as proved by the experiments of Zhang [17].

2.1.2 Adaptation of the ALTP as a Sensor

Seeing the sensitivity of the ATLP film to laser or any source of heat flux, it was adapted to be used as a sensor. It is presently a well-established sensor in the field of UV and light detection. Due to the fact that the distance the charge carriers need to travel in the so called thermocouple junctions of the film is much smaller than any macroscopic thermocouple junction presently available, the response time of the sensor is significantly faster than a thermocouple. This phenomenon makes the ALTP uniquely suited for measuring high frequency fluctuation in heat flux which are very commonly found in environments with high speed flows such as combustors,

turbines and nozzles. This adaption of the ALTP film to measuring heat flux in such environments is the scope of this work.

Knauss et al [19] were the first people to document the use of ALTP for high speed flows. The ALTP was commercialized by Fortech GmbH. The schematic of the available sensor is shown in Figure 2.4.

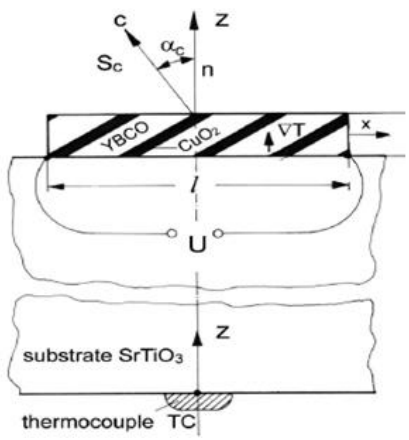

Figure 2.4 Schematic of the ALTP sensor with the electrical connections and thermocouple position [16].

The sensor consists of the basic epitaxial inclined $YBa_2Cu_3O_{7-\delta}$ film deposited on a $SrTio_3$ substrate, though other substrates have also been used and one such substrate, magnesium oxide MgO, is explored as an alternative in this work for high temperature environments. The sensor is instrumented with two electrical contacts on the sides of the film, thus the x-component of the electric field generated is measured for a temperature gradient in the Z axis according to the coordinate system shown in Figure 2.4.

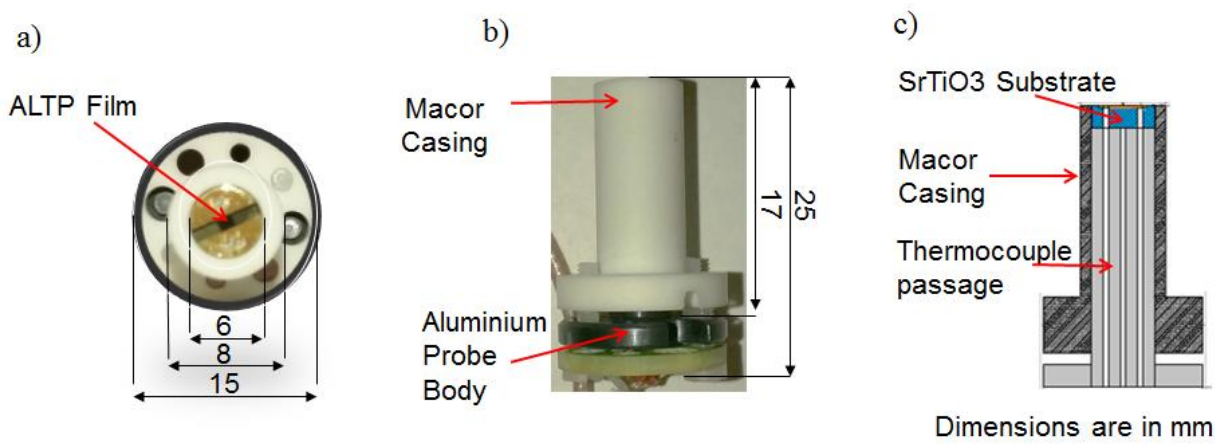

Figure 2.5 Photos of the ALTP probe, a)Top view of the ALTP Probe with the film position highlighted, b) Front view of the ALTP probe showing the different layers of the probe body, c) Schematic of the inner cut section of the ALTP probe.

The sensor substrate is mounted on a cylindrical aluminum stem and is glued using a thermally insulating epoxy. The aluminum stem has three holes machined in it, two of them allow the passage of wires for the electrical contact on the film and these wires are then soldered on a mica plate mounted on the back of the aluminum stem which opens up into a flange at the end with tapped and untapped holes. Nylon screws are used for these holes and two screws hold the mica plate with the aluminum stem. The electrical contacts with the film are made of brass and the electrical wires are 40 AWG made of copper. The third hole at the centre of the aluminium stem forms a passage that ends at the back of the substrate. A thermocouple can be mounted in the passage to measure the temperature at the back end of the substrate, referred to as the back substrate temperature in this work. The aluminum stem and the substrate-film are housed inside a cylindrical housing made of macor, which is a machinable glass ceramic made by Corning Inc. This housing is also clamped to the aluminum flange using nylon screws as described before. The aluminium stem is 6mm in diameter with the macor housing of 1mm thickness, bringing the total diameter of the probe as 8mm. The macor housing provides thermal insulation on the sides due to its very low thermal conductivity of around 1.46W/mK at 25°C. This allows us to treat the heat flow inside the sensor probe as one-dimensional with minimal distortion due to this assumption. The active area of the sensor is much smaller than this value, as shown in Figure 2.5. There are two available sensors with 2X1mm active area and a 5X1mm active area that is coated with a SiO_2 protective coating.

This allows the sensor to handle much larger heat flux, but it decreases the response time to 100KHz. The smaller sensor is rated for a response frequency of 1MHz.

2.2 Review of Heat Flux Calibration Techniques using Atomic Layer Thermopile film

2.2.1 Static Calibration through exposure to Radiation

As mentioned earlier, the discovery of the ALTP film was made when it was exposed to light pulses and it quickly became a standard sensor for light detection applications. The most common method for calibrating the sensor output for light detection is to pulse it with light at different intensities and record the output voltage. Extensive testing is done with carbon dioxide CO_2 lasers by the Fortech GmbH and they have come up with an absorption coefficient of 0.86 [19] of the total power for the CO2 laser wavelength broadband of 9.4 to 10.6 µm. Other works using the ALTP sensor have traditionally all relied on using the laser calibration technique, including multiple studies by Roediger [16][20], Jenkins[27], Knauss[19], Lejsek[21] who applied the technique to measure heat flux inside SI engines with direct injection of gasoline and it has also been utilized by NASA Langley's Research centre by Kegrise and Rugfer[22] in their study of second mode instability waves. The typical arrangement for this type of calibration includes a CO2 laser that is passed through an optical system to obtain a known intensity of light on the surface of the sensor. A system to measure the power of the beam is also present either in parallel to the main path and the beam is sent by a splitter or by positioning it in the middle of the beam path. Figure 2.6 shows the calibration setup used by Roediger [16].

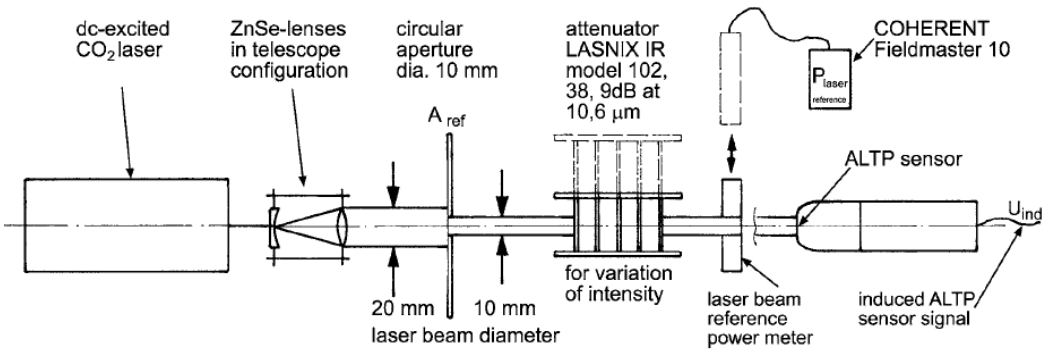

Figure 2.6 Typical Laser calbration setup for static calibration of ALTP [16].

Extensive test done by various groups have shown the linear nature of the ALTP for such type of calibration from the mW/cm^2 to W/cm^2 regime. Though higher power lasers are generally pulsed, the most common laser used are continuous wave(CW). They can be pulsed using mechanical shutters or with function generators to provide pulse jumps in heat flux.

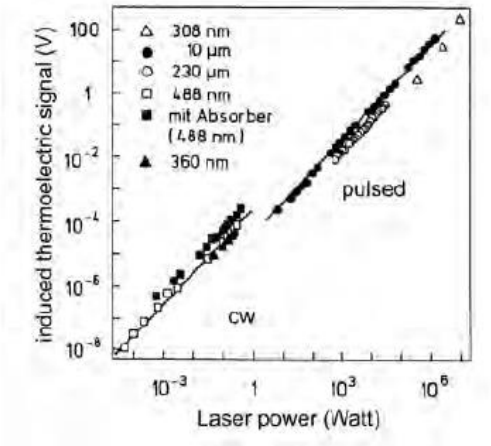

Figure 2.7 Test results for ALTP film showing linear nature over broad range of heat flux [16].

One of the fundamental drawbacks that can be seen in this method is that the surface properties of the film are generally unknown and the absorption percentage changes with the wavelength of light used. Also due to the nature of light itself, in general laser beams are Gaussian in nature and hence their intensity distribution is not really uniform. To generate higher power, pulsed lasers are generally used, where again the material is exposed to multiple low powered pulses in a very short duration to achieve very high power intensities. However, since it is not possible to know or isolate the power of individual pulse for a pulsed laser, it is important that the pulse duration is much faster than the resolution of the senor so that the sensor feels the entire laser power as a single pulse.

Other methods of using radiation apart from using lasers have also been employed to calibrate heat flux sensors. Pullins [26] used a cavity radiator using a cold and hot plate separated by an air cavity to calibrate a custom designed thermopile for heat flux measurement. The effect of convection was minimized but not completely removed.

2.2.2 Dynamic Calibration through laser exposure

Dynamic calibration of the ALTP is generally carried out using high speed laser diodes, which are pulsed using an external pulsing circuit or function generator. The laser light can also be pulsed using a mechanical shutter, but that limits the maximum frequency. The light is split between the ALTP and another light sensor, usually a photodiode and the two signals compared. Figure 2.8 shows the dynamic calibration setup used in the work of Kegrize.

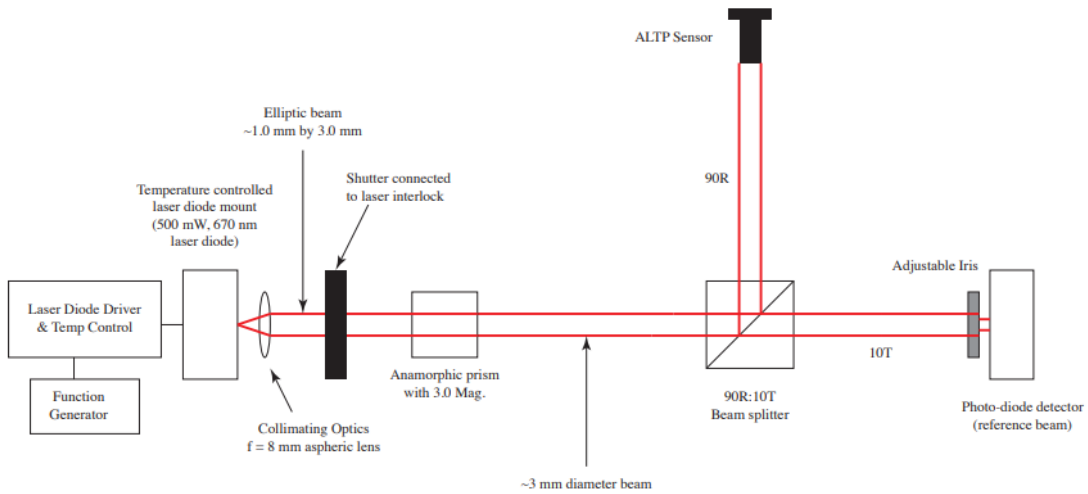

Figure 2.8 Typical Setup for dynamic calibration of ALTP [22].

2.2.3 Calibration of Heat Flux Sensors in a Convective Environment

The use of radiation is standard practice for calibrating heat flux sensors, however in practice there are a lot of applications where the sensors are used where heat transfer through wither conduction or convection dominates. Since the scope of this work deals primarily with convection driven heat transfer we will focus on the calibration methodology that can be used for convective environments. Holmberg [23], from the National Institute of Standards and Technology came up with a methodology of using a heated plate of pure copper that will be exposed to cold laminar flow. The plate would be heated using heaters and by controlling the amount of power input to the heater, they could change the amount of heat flux. To compensate for peripheral losses of heat, the plate was divided in six different regions with a heater for every region and these heaters could be individually controlled to give a uniform temperature profile over the plate. With their initial

configuration they were able to achieve 10% relative uncertainty in their measurement. This design was further revised by Holmberg[24] to being down the total uncertainty in the facility for the reference heat flux measurement to less than 3%. This also included a more thorough analysis of the several heat loss pathways and how they could be eliminated. This methodology compares the heat flux measured by the sensor to be calibrate with a reference zone where the heat flux is calculated in the absence of disturbance from the sensor itself.

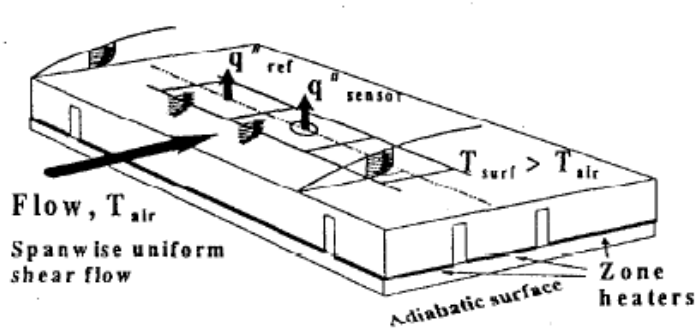

Figure 2.9 The NIST convective heat flux calibration test plate [24].

The second generation of design had foil heaters that on the back along with backing heaters further down to prevent any heat loss along the depth of the test plate. It also followed the approach of semi isolating the areas of interest from the rest of the surrounding and using individual heater for each section to maintain constant temperature. The position of the sensor in the NIST wind tunnel is right where the flow should transition from laminar to turbulent, giving the most value of heat flux. While the flow in this case was parallel to the plate, Borell[25] carried out the calibration of a Gardon type thin foil heat flux guage by keeping the plate perpendicular to the flow to provide more heat flux since the sensor was located now at the stagnation point of the flow.

2.2.4 Heat Flux Measurement in Turbomachinery

Heat flux is an important property for turbomachinery components and it is one of the more difficult parameter to measure with low uncertainty and high frequency. Several methods have been developed over the years to measure heat flux over turbine components such as blades, the inner walls of the hub and shroud etc. The most common methodology applied relies on the

measurement of temperature on the surface from which the heat flux is calculated. The calculation of heat flux is itself a source of uncertainty since no analytical solution exists to calculate heat flux with step change in temperature which is the case for most wind tunnels testing turbine components especially in blow down type wind tunnels. The semi-infinite solid assumption is widely used for the analytical solution. Another major development in this field was the use of thin films. These thin films are generally resistor type temperature sensors, where a resistance sensor is deposited on an insulating thin film. When the material is exposed to flow, the resistance of the deposition changes proportional to the temperature. Based on this temperature and the properties of the film and the material properties of the backing material, the total heat flux can be calculated. Both analytical solutions and electrical circuits have been used to convert this temperature signal to heat flux. Single layer substrates have used electrical circuits and amplifiers that provide almost $\sqrt{f}$ gain for the high frequency heat flux as evident by the works of Meyer [28] and Oldfield [29]. Doorly [30][34] demonstrated the conversion of a frequency boosted signal from a thin film guage to the corresponding heat flux. Ainsworth [31], applied this methodology for multilayer thin film gauges for rotating turbine components.

Saavedra [1] developed a one-dimensional numerical unsteady state solver to overcome the semi-infinite assumption and tracked the temperature at a known distance from the flow exposed surface. Knowing the two temperatures, the solver can then interpolate the wall heat flux more accurately than the with the semi-infinite solution.

Thus calculating heat flux by measuring the surface temperature is an established methodology in turbomachinery experiments. Other techniques used to measure temperature has included temperature sensitive paint [32], infra-red thermography [33].

The uncertainty on the heat flux calculation using the methods described here depends on the properties of the material used to determine the heat flux and also on the assumption used to calculate the heat flux.

2.3 Calibration Through exposure to radiation

2.3.1 Description of Experimental Setup

The standard for calibration of Atomic Layer Thermocouple type sensors has been exposure to radiative heat flux using a laser or any other concentrated high energy light source. This methodology is relatively straightforward and does not require complex post processing of the data. The general concept for this method of calibration is that the sensor is exposed to the chosen radiation source and the power output of the radiation source is known. The sensor response is compared with this known input heat flux. The measurement of the power from the radiation source maybe taken either by measuring the input power to the radiation source circuit or by measuring the power of the beam using a power meter. This is the method that has been utilized by all users of the ALTP sensor system before this work namely Roediger et.al [16] and Knauss [19]; For this work, a continuous wave laser of 532nm was used as the radiation source. The laser output power was measured using a 'Coherent Power Max PM3', power meter. The power meter was kept in the path of the laser and after a reading was taken, it was removed, and the laser path was blocked next by a high-speed shutter. The shutter was designed to open and expose the sensor for 100ms before closing, effectively giving pulse heat flux jumps to the sensor and the signal was recorded. The laser beam was a Gaussian beam, which implies that the intensity varied as a Gaussian distribution around the centre of where the laser beam impinged on a surface and subsequently reduced in intensity as one goes further from the centre of the beam. The nature of light means that there is no actual boundary for the end of the beam spot since the light intensity will go on till infinity, which leads to the issue of not knowing the spread of the heat flux source over the surface the laser beam impinges upon. To make sure that almost all the output power of the laser, it was decided to focus the laser beam such that the surface of six-sigma distribution of light intensity, i.e 99.84% of intensity, has a diameter that is smaller than the outside confines of the working surface of the ALTP film. The calibration assumes that the signal generated from the sensor is the area average of the film active surface hence the local temperature gradients generated due to the concentration of the heat flux source are neglected. The laser was focused to a beam diameter of around 1mm centered around the centre of the film. This is different from the method used by other authors with experience with thin film sensor calibration where they diverged the

beam so that the entire surface of the film was within the six-sigma boundary of the laser beam and then proceeded to assume that the heat flux distribution inside the boundary and hence the light intensity distribution was uniform inside the six-sigma boundary. The effective area for the calculation of the heat flux input is still taken as the active area of the sensor film, i.e 5X2 mm for sensor 1 and 2X1mm for sensor 2.

The experimental setup consisted of a CW laser and all accessories required to power it, a high speed mechanical shutter, power meter and 2 sets of converging lenses to focus the laser beam to required diameter at the location of the sensor. The senor was housed in a clamp and placed in the laser beam path with the active film surface facing the laser path, the position was adjusted such that the laser beam centre coincided with the ALTP film. To achieve the alignment, the laser was operated on the lowest power output to avoid heating or accidently damaging the ALTP during the alignment. A thermocouple monitored the back-substrate temperature of the ALTP probe even though the exposure time of the radiation was very short and a measurable increase in the substrate temperature was not predicted. Two sets of lenses were used to focus the laser beam on the centre of the ALTP film and reduce the diameter of the beam to diameter of 1mm. The diameter of the beam was checked by taking an image of the beam on a Closed Circuit Detector(CCD) Camera and counting the number of illuminated pixels and using that pixel count to convert to length. A LABVIEW program was used to control the shutter and acquire signal from the signal. The ALTP signal was amplified using a two-channel amplifier, 1 channel with a programmable fixed gain over all frequencies from DC to 100Khz. For this calibration the amplification gain was set at 100. The 2nd channel of the amplifier was to amplify the high frequency component of the signal by a gain of 5000 from 17Hz onwards to 1Mhz. The nature of this calibration method implied that no high frequency signal should be generated during the steady part of the experiment. However, several orders of frequencies will be excited during the opening and closing of the shutter as the film will be exposed to sudden steps in heat flux. These frequency excitations are clearly visible in the signal spectrogram. A FPGA data acquisition system was used as the analog to digital converter for this case.

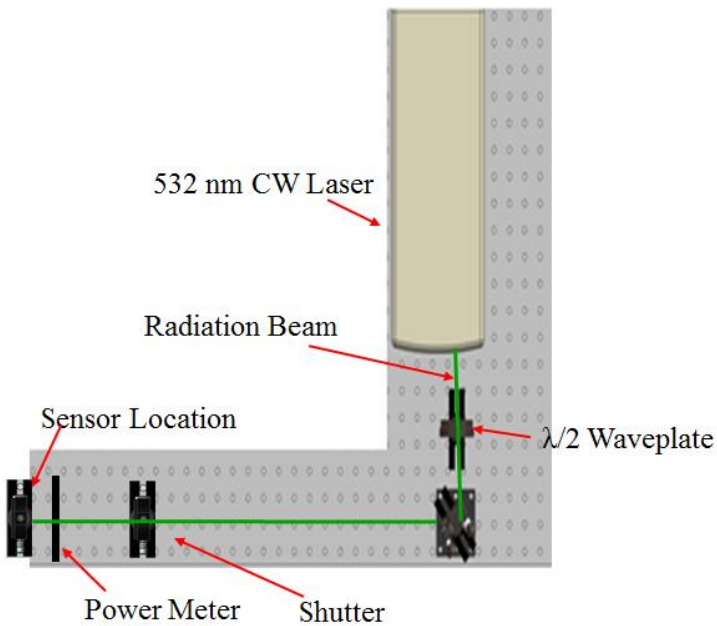

Figure 2.10 Schematic of Experimental Setup for calibration through exposure to radiation, the schematic shows the position of the mechanical shutter, CW laser and the location of the sensor holder and the power meter with respect to each other .

The acquisition rate of the system was 100KHz. 8 points of increasing power were decided on and the laser intensity was changed accordingly. Once the set power was confirmed by the power meter, it was removed from the laser path and the shutter was open and closed

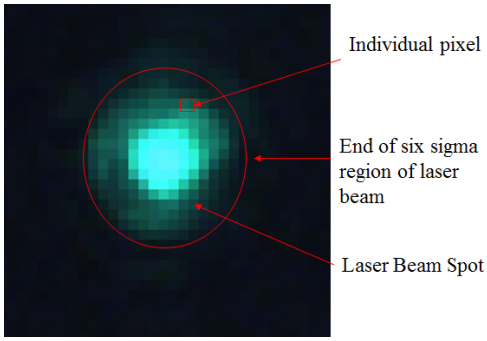

Figure 2.11 CCD image showing laser beam spot and pixels which were used to estimate the beam diameter.

The calibration was run on both types of ALTP sensors present, the slower one with frequency response of upto 100Khz and the faster response sensor. The setpoints of the power were changed accordingly since the faster response sensor has smaller sensitivity and a lower damage threshold.

2.3.2 Uncertainty Estimation

One of the major problems associated with the calibration using the exposure to radiation is the accurate estimation of the actual heat flux input to the film without accurately knowing the film surface emissive properties. Since the input radiation is either transmitted through or reflected along with being absorbed by the surface and acting as a heat flux input, the accurate estimation of the heat flux input requires precise knowledge of the surface properties. This uncertainty in the emissive surface property estimation forms the biggest contributor in the uncertainty of the calibration. Another important source of uncertainty is the uncertainty associated with the measurement of the input power using the power meter. At best the uncertainty is the resolution of the digital power meter. Due to the packaging of the sensor and the probe it is difficult to measure the surface properties. Since the substrate is opaque, it is hard to estimate the transmissivity of the film and the effect the laser has on the signal by heating the substrate. Also there is no way of accurately measuring the surface temperature of the ALTP film. Since the exposure time in such calibration is very low, there is no measureable change in the back substrate temperature, however it cannot be concluded based on this that there is no increase in the temperature in the film itself. Since the signal generated is based on the temperature gradient across the ALTP film, it is good to have an estimate of this gradient and the only measurement that we have for the prediction of this gradient is the temperature of the surface at the back end of the substrate, which in this case will not rise measurably.

The uncertainty of the power meter is 2%. It was calibrated for 514nm wavelength and a wavelength of 532 nm was used, the spectral compensation accuracy is 1.5%. The linearity with power is 1%, but the range of powers tested were low. So using the uncertainty estimation from Moffat[3], we get an uncertainty of 2.5% on the accuracy of the measured power. The uncertainty in the voltage measurement is the resolution of the data system, in this case it was 20 microvolts for the noise level.

2.3.3 Results

From the radiation exposure, we get jumps in the signal from the ALTP, when the shutter is opened. The mean value of the signal depends on the power of the exposure. Different exposure

windows were used and the mean from each compared. As seen in Figure 2.12 the jumps are uniform.

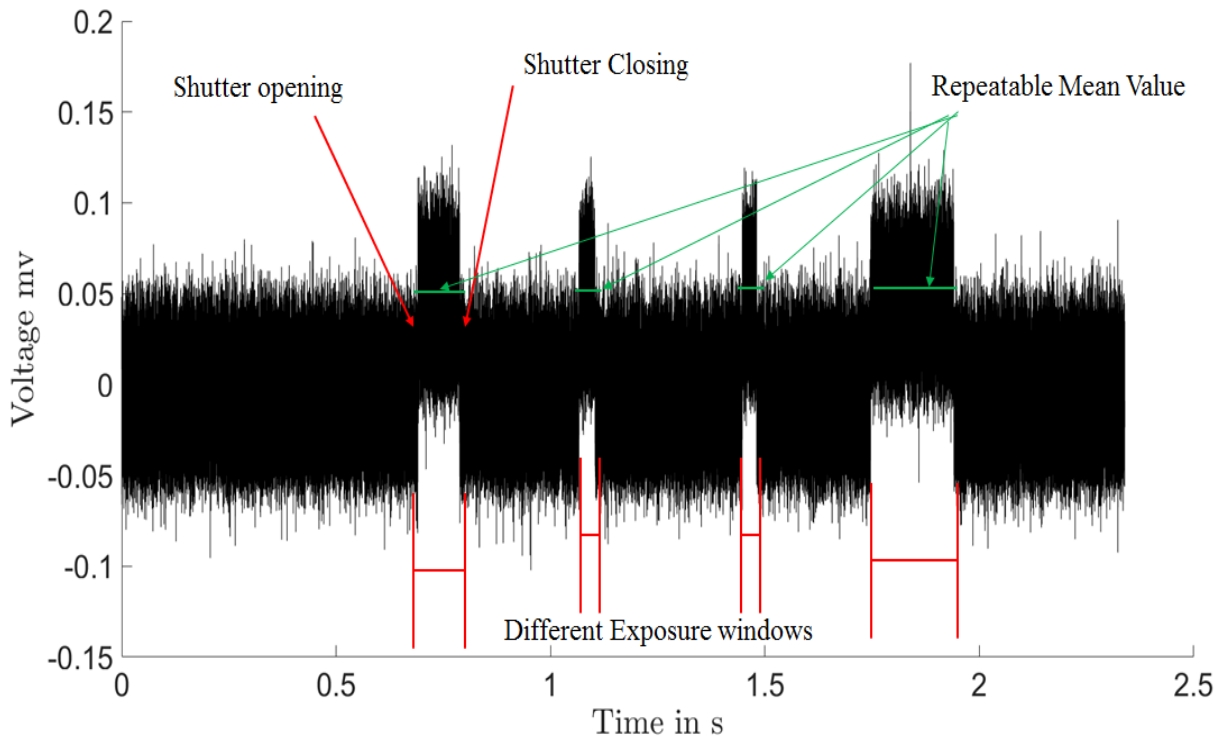

Figure 2.12 ALTP signal output at given laser power.

Base on the different laser powers tested, a calibration line of ALTP voltage signal vs input power based on the area of the film was plotted for both ALTP sensors. The correlation square values for both are 0.997662 and 0.98771 with a sensitivity of 76µV/W/cm^2 and 36µV/W/cm^2. The correlation square values confirm that the behavior between the signal and the power input is linear. The average standard deviation around the mean is 120 W/m^2 for ALTP-1 and 1917W/m^2 for ALTP 2. Adding the uncertainty from the uncertainty analysis, the average uncertainty in the reading is 4% for ALTP 1 and 100% for ALTP 2. The powers tested for ALTP 2 were very low.

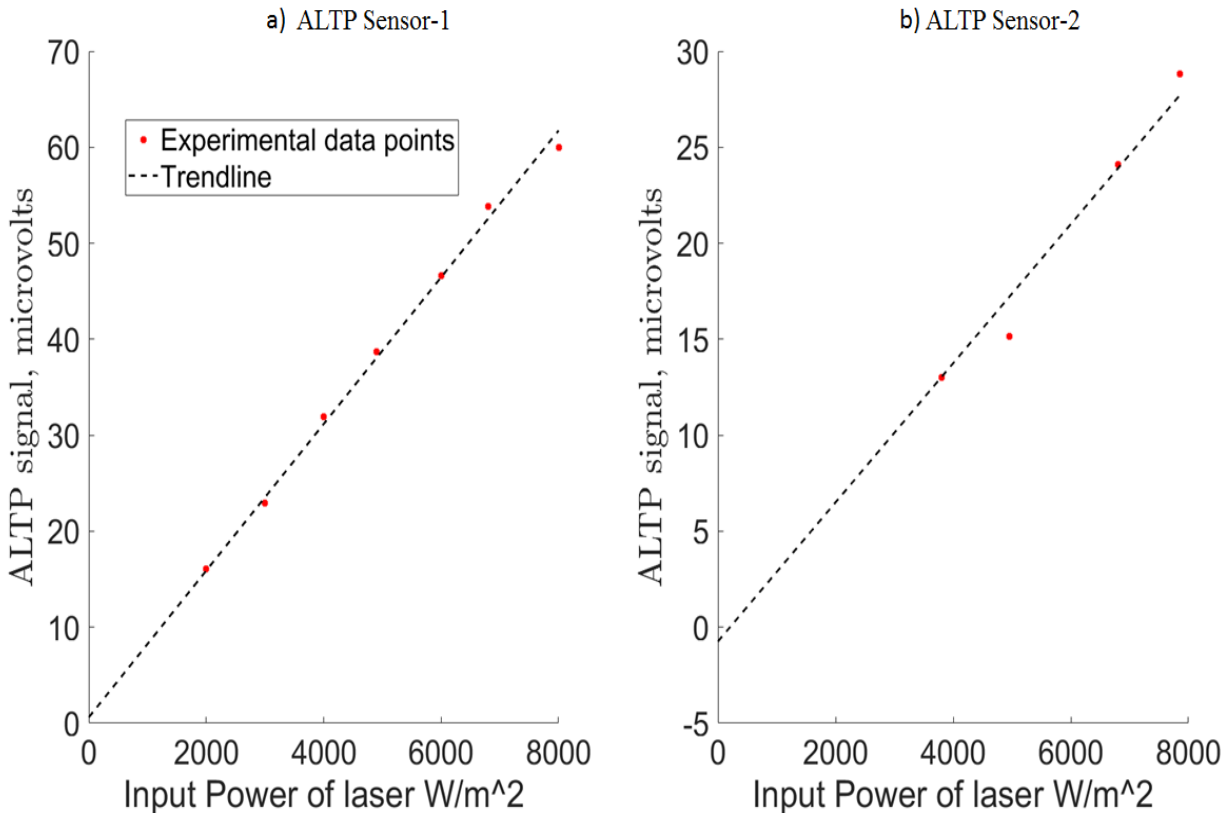

Figure 2.13 Calibration curves showing linearity between voltage and input heat flux for two ALTP sensors. a) ALTP sensor 1 has higher sensitivity but a slower response upto 100KHz. b) ALTP sensor 2 has lower sensitivity and lower damage threshold but a higher frequency response upto 1MHz.

Assuming a perfectly linear behavior of the ALTP, if we evaluate the slope and intercept uncertainty and then based on the linear relation compute an uncertainty relation for The relative heat flux uncertainty, we find that due to its very small values, both sensors have very high uncertainty in their slope and offsets. The slope uncertainty for the first ALTP is 5% but 348% for the intercept. For ALTP 2, the slope uncertainty is 11%, but 175% for the intercept. The derivation of the formulas used to compute this uncertainty is given in 2.5.2.

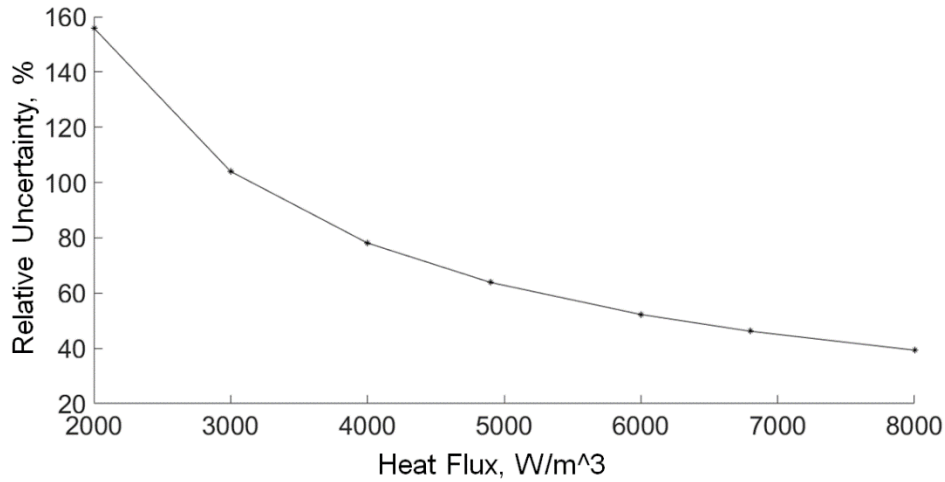

Figure 2.14 Relative uncertainty with heat flux based on slope and intercept uncertainty.

The spectrogram of each signal was also looked at to check the excitation of frequencies when the sensor is exposed to laser. The spectrogram was computed by averaging 2048 samples, with 75% overlap in segments with a hann window of length 2048 and the given sampling frequency of 100kHz. The spectrogram confirms the change in the signal with the opening and closing of the shutter. There is a sudden excitation of several frequencies as the signal jumps from one mean level to the other. Based on the time window of the jump, we can show that the ALTP within 100 µs to respond to what is a pulse signal.

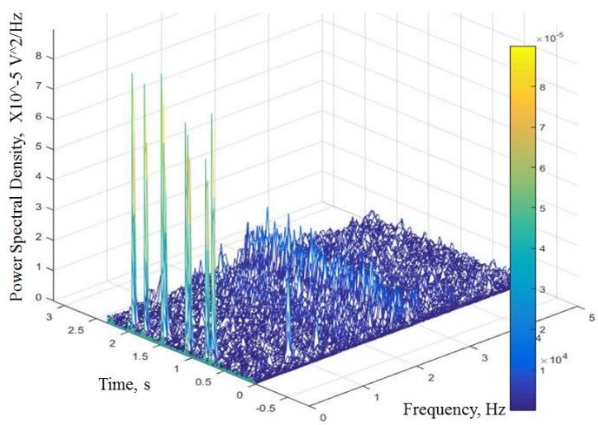

Figure 2.15 Power Spectral Density spectrogram of the ALTP signal when exposed to laser burst. Each jump in PSD is an indication of either the shutter opening or closing.

2.4 Calibration by Electrical Measurement

2.4.1 Description of Experimental Setup

A method for better estimation of measurement uncertainty with the ALTP that are associated with a flow environment, which is the ultimate objective of this work, is developed in this section. This methodology tries to generate a steady heat flux environment by exposing an isothermal flat plate to cold flow. To achieve this, a flat polished copper plate is taken, with slots made into it for a test coupon and a reference coupon. The test coupon has a hole in the centre where the ALTP is mounted. The reference coupon is completely smooth. Both these test coupons are separated from the surrounding copper plate with an epoxy bridge of very low thermal conductivity. Copper is chosen because of its high thermal conductivity, so that there are very low thermal gradients present in the lateral direction in the test coupons. The test coupons are surrounded by another copper plate to further reduce lateral temperature gradient by keeping the outer copper plate at the same temperature as the test coupons. The entire copper plate is then surrounded by laminate of paper impregnated with a resin, known as phenolic sheet. The sheet provides excellent electrical isolation along with low thermal conductivity. It is easy to work with as it can be machined with standard machine tools rated for aluminum. One side of the polished copper plate is exposed to the flow and on the other side foil heaters are mounted to heat the plate. Each coupon has its own individual foil heater and its own power supply. The outer copper plate has three foil heaters mounted, all three driven by the same power supply in a parallel configuration. This is done for ease of control during operation. Eight Resistance Temperature Detector's (RTD's) are mounted on the back of the plate to measure the temperature at different points in the plate.

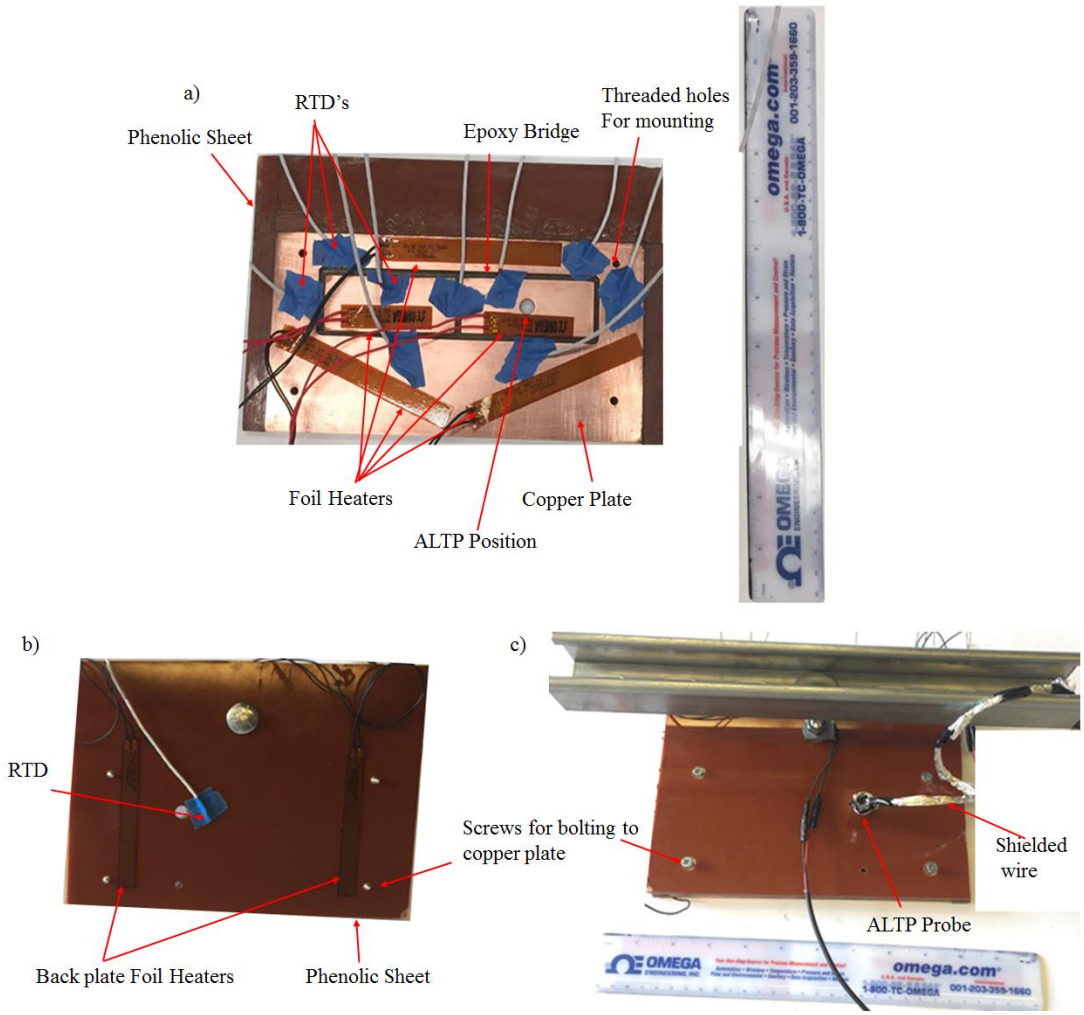

Figure 2.16 Layout of test article. a) Assembly of copper test plate with the foil heaters and the position of the RTD's b) Assembly of the backing phenolic sheet showing the location of foil heaters and RTD. c) Back view of the backing phenolic sheet showing the location of the ALTP probe.

Figure 2.16 a shows the arrangement of the test coupon, the position of the foil heaters and the RTD's used to measure temperature. On the back side of the copper plate with the foil heaters, a second layer of phenolic sheet is bolted through four threaded holes on the copper plate. On the inner side of this phenolic sheet there are mounted two other foil heaters to reduce the temperature gradient in the depth of the test article. A RTD mounted on the phenolic sheet gives the temperature of the back plate and allows us to estimate the losses in the depth of the test article.

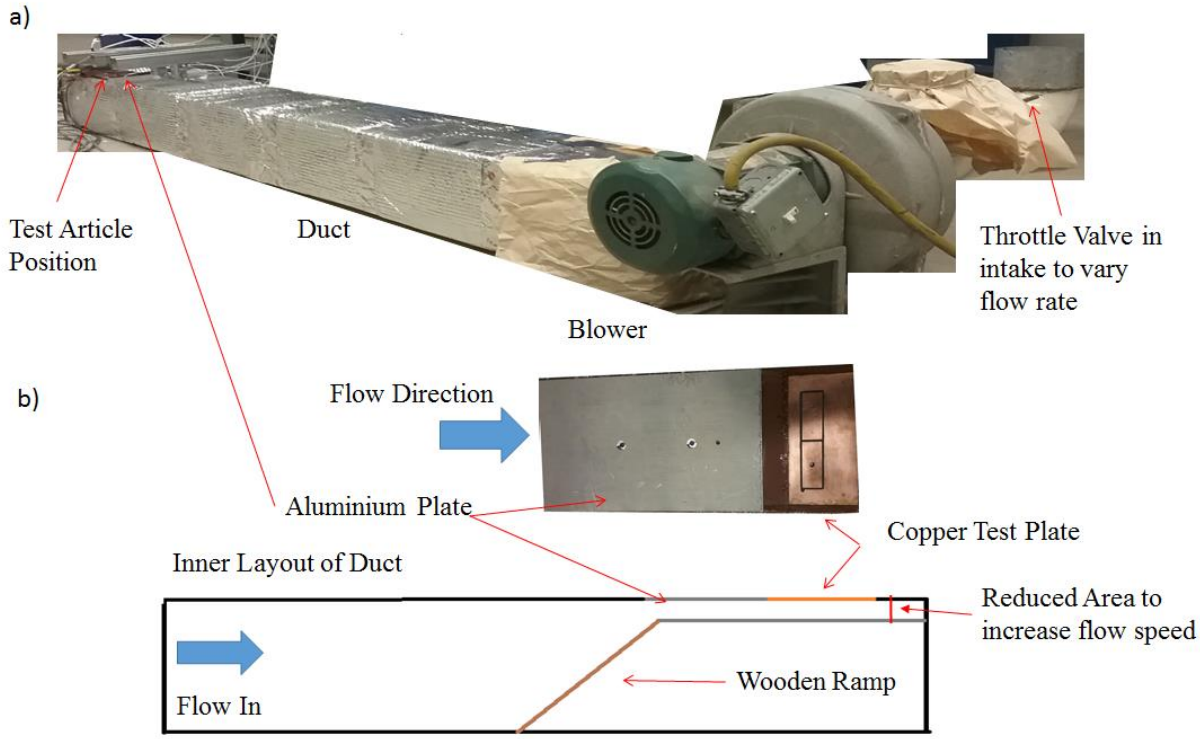

Figure 2.17 a) Layout of the test section showing the arrangement of the blower and location of the test article. b) The inner schematic of the duct.

The test article is placed inside an insulated duct with a blower at the end. The blower has a throttle valve which allows changes in flow velocity. A ramp, as shown in Figure 2.17b), is present in the duct to reduce the area near the test article and increase the velocity at the point of measurement to increase the wall heat flux. Sufficient length of the test article was present from the ramp till the test article to allow for fully developed flow.

A series of variable and adjustable power supplies were used to power the foil heaters, and the input power was calculated by measuring the current in the circuit and by measuring the voltage across the junctions of the foil heaters, rather than the junction of the power supply. The data acquisition was done using NI 4357 cards for the RTD's and Agilent voltmeters for the voltage and current. The ALTP was read using NI 6363, high frequency cards with custom built two channel amplifiers. The current was indirectly measured using a current shunt which generates a voltage drop across its terminals that is proportional to the current flowing through it. This is done

to reduce the error associated with current measurement by preventing any new load being added in the circuit and measuring current through a circuit in parallel to the current circuit.

Different voltages were applied to the copper plate and the flow was initiated. The system was allowed to achieve steady state, that is when the temperature of all RTD's come to a plateau. A thermocouple mounted at the back of the ALTP measured the temperature difference between the copper plate and the ALTP substrate. The voltages of the foil heaters were varied till very small temperature gradients were present in the copper plate. At this point the ALTP readings were taken.

2.4.2 Uncertainty Estimation

In steady state, the amount of heat that was being inputted to the copper plate would be equal to the amount of heat being carries out by the flow. Based on the assumption of steady state, the entire test setup was analyzed to estimate the different heat flow path and how much contribution they have compared to the primary heat flow path of interest, i.e the heat flowing from the foil heater to the copper test coupon to the flow. Figure 2.18 shows all possible heat flow path.

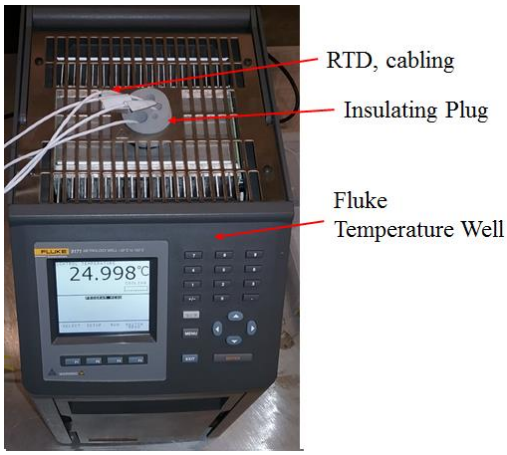

Figure 2.18 Arrangement of the Fluke constant temperature well and the RTD's during calibration.

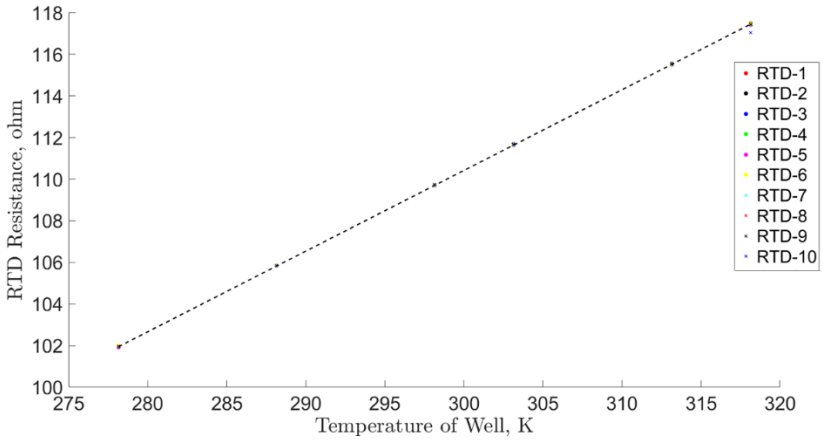

Figure 2.19 Calibration curve of the RTD's showing sensor resistance with well temperature.

For the uncertainty, it all the possible heat paths were analyzed. For the lateral heat conduction, steady state heat loss was assumed, and the temperature difference being the uncertainty in the RTD values. For vertical conduction through the metal screws in the plate, an estimate was calculated based on the screw material and dimensions. The values are tabulated in table 1.

The uncertainty was calculated by finding the total change in heat flux due to each conduction path. The total uncertainty in each conduction path was calculated using the assumption of Moffat[3].

Table 2.1 Pre Experiment Uncertainty Estimation.

	Mean Value	units	Uncertainty	Direction	Sensitivity
Lateral Conduction					
Temperature Difference	0.15	K	0.353	X(L)	1
	0.15	K	0.353	Y(W)	1
Length	0.076	m	0.00001	X(L)	1
Width	0.031	m	0.00001	Y(W)	1
K epoxy	0.2	W/mk	0.05	X(L)	1
	0.2	W/mk	0.05	Y(W)	1
Gap length	0.001	m	0.00001	X(L)	1.01
	0.001	m	0.00001	Y(W)	1.01
Epoxy Height	0.00635	m	0.00001	X(L)	1
	0.00635	m	0.00001	Y(W)	1
Area	0.0022	m^2	0.00141		2.367
Mean Value of heat loss		W		Q1 X(L)	0.014
Mean Value of heat loss		W		Q2 Y(W)	0.006
ΔR_x	0.034				
ΔR_y	0.014				
Vertical Conduction					
Q from FEA	631.9	W/m2			
Generated Temperature Difference	0.141	K			
Heat from Temperature Difference	997.7	W/m2			
Length of bolts	0.00635	m			
Thermal Conductivity	28.5	w/mk			
ΔR_v	0.578947				
Loss Through RTD Wire					
RTD Wire Dia	0.00405	m	0.001	1.032	
PFA Thermal Conductivity	0.182	W/mk	0.042	1	
ΔR_{RTD}	0.34				
Mean Loss in Heat		0.047	W		
Error in heat loss		0.037	W		
Heat Input Value		1.37	W		
Sensor value at mean		1.34	W		
Min sensor value		1.28	W		
Error in sensor reading		4.66	%		

2.4.3 Results

The results from this experiment were not conclusive. As can be seen in Figure 2.20, the data points are very scattered and no proper trend is available. The spread is much greater than that found using the exposure to radiation experiment.

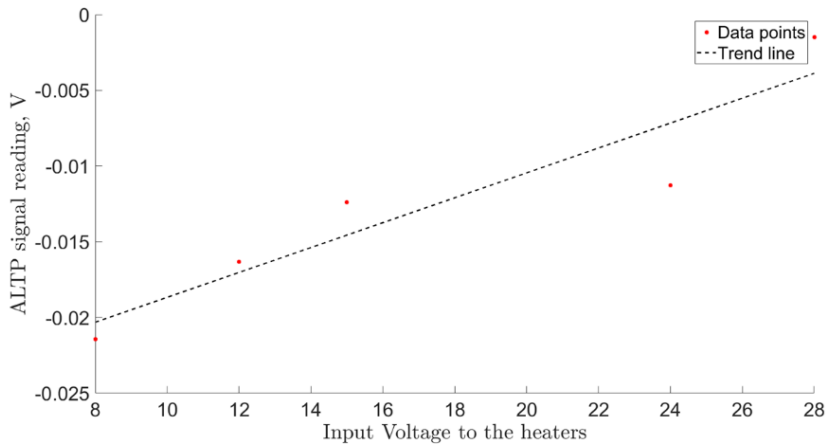

Figure 2.20 Results of the calibration showing the ALTP voltage signal with input power in terms of heater input voltage.

The heat flux values measured was then compared with the analytical solutions for a flat plate boundary layer for laminar and turbulent flow using the flow properties measured during the test. This was done to check is the overall trend in the heat flux measurement match what should be happening. It is assumed that the actual heat flux value should lie in between the laminar and turbulent conditions since the flow was not laminar, nor was it completely turbulent. However as seen in Figure 2.21, the measured values differ significantly from the analytical relations. This slopes of the turbulent and laminar solutions are much lower than the measured data points. So this experiment was considered inconclusive and the possible reasons for this behavior was analyzed.

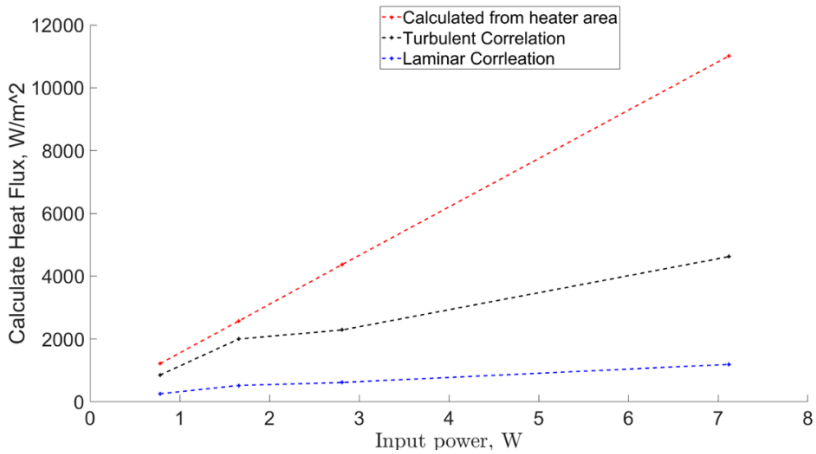

Figure 2.21 The trend of the empirically calculated heat flux based on flow parameters wall temperature for purely laminar and turbulent flow in relation to the heat flux input to the heater.

2.4.4 Limitations

There are several limitations in the design and execution of this methodology. Firstly, for steady state conditions to be reached, the system takes a long time. The data was collected after runs of 6hours long, but that time was not sufficient enough to reach steady state since the temperature of the plate was still changing. Another major factor was the presence of the Macor layer around the ALTP sensor. The insulating layer not only increased the time it takes to reach steady state. The presence of the insulating layer also ensures that the temperature at the film is much different from the temperature of the plate. This invalidates our assumption of uniform temperature of the flow exposed surface of the plate and no comparison between the reference coupon and the ALTP reading can be made within a reasonable degree of accuracy. A new approach for calibration in a convective environment was needed.

2.5 Calibration using Heat Flux calculated by Transient Convective Heat Transfer

2.5.1 Description of Experimental Setup

Due to the limitations, discussed in the previous section, of the method of calibrating heat flux sensors in steady state environment, another methodology was investigated, where sudden transient in flow were present and the sensors were evaluated with respect to another type of

measurement which is more accurate than heat flux directly, namely temperature. This methodology is a secondary calibration method since we are evaluating against another sensor. This technique was carried out in the linear wind tunnel of the Purdue Experimental Turbine Aerothermal Lab(PETAL), based out of Zucrow Labs. This experiment involved the complete measurement chain that will be used for measurement of heat flux in supersonic flow. This includes the data acquisition system used and the length of the measurement wires involved. Since the raw signal of the sensor is of the order of microvolts, the length of the cables and the setup of the data acquisition system (DAS) in general, is of prime importance to ensure we have accurate readings and minimum distortion of the signal.

The linear wind tunnel at PETAL has a cuboidal test section of cross-section of 230X170mm and length of 531mm. (check dimensions) The test section is preceded by a settling chamber that is designed to damp out all oscillations and eddies in the flow formed due to the upstream piping. The settling chamber discharges the flow radially at its inlet into a large volume compared to the inlet pipe diameter. The flow is passed through several layers of honeycombs and screens to straighten the flow before it is accelerated through a Bezier curve based nozzle that is designed to channel the flow from a circular cross-section to the rectangular cross section of the test section. The flow is provided by $36m^3$ of compressed dry air tanks which are pressurized to 150 bar(2200psi). The flow is passed through a heater and then enters the test cell housing the linear wind tunnel. The facility is capable of handling both cold and hot flows upto 700K. The flow inside to the test section is controlled by high speed butterfly valve that is designed to open in 100ms, giving rapid transient to the flow. Another butterfly valve purges the air to the atmosphere when flow is not required inside the test section, before the flow achieves test conditions. The control logic for sudden discharge is designed that the linear butterfly valve opens 100 ms after the purge butterfly has start to close.

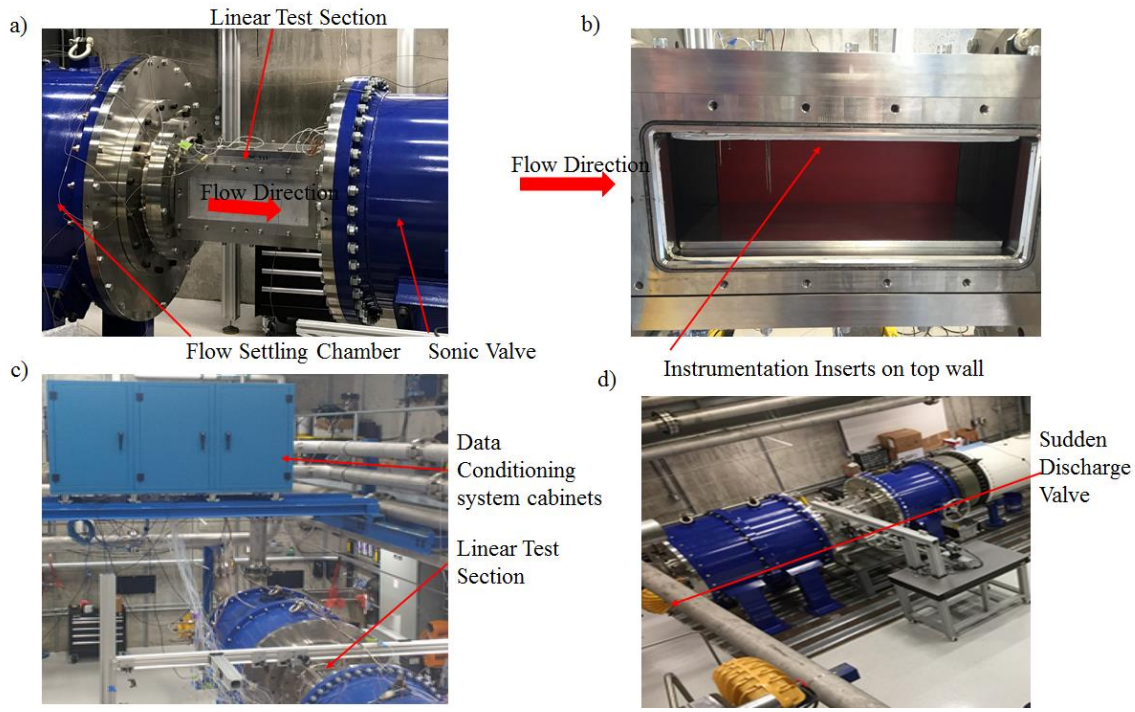

Figure 2.22 a) The linear wind tunnel test section at PETAl b) Opened linear test section showing the location of mounting of instrumentation. c) Location of the cabinets containing all conditioning system with respect to the wind tunnel. d) Layout of the linear wind tunnel.

As shown in Figure 2.22 c), the data conditioning and analog to digital converters are mounted inside a series of temperature controlled cabinets mounted on a rail or on the wall, isolated from the ground to reduce the effect of vibrations on the data signal. Downstream of the linear test section, there is a sonic valve which can control the Mach number in the test section by choking the flow in the valve and setting the area ratio which sets the Mach number in the test section. All the flow is purged inside a vacuum tank, which is sealed during vacuum operation or can be kept open when discharging to atmosphere.

The linear wind tunnel has a modular instrumentation insert system, where different inserts containing mounting fittings for different instrumentation, can be installed depending the requirement of the test campaign. For this test, an insert plate was prepared to mount the ALTP sensors along with the surface thermocouples.

Surface thermocouples are thin wire thermocouple with their junction encased within two layers of kapton tape, which prevents the thermocouple coming in contact directly with the metal surface and hence prevents generation of another junction with the surface of interests and it also allows

the thermocouple to attach to the surface. The diameter of the wire is 0.127 mm which is small enough that it does not protrude significantly in the flow path. Surface thermocouples are mounted on the insert plate on the side exposed to flow and also on the outside which is exposed to ambient conditions. Multiple thermocouples are used to ensure stability in temperature and also to provide redundancy in case one of the thermocouples break or come lose during operation. The thermocouple wires are passed to the flow side through holes drilled in the plate and the wires are sealed using Swagelok fittings. To mount the ALTP in the insert, a hole was drilled equal to the outer diameter of the macor sheath of the probe, which opens into a rectangular pocket with a groove around the hole for an o-ring. A silicon o-ring is used, with a temperature rating of 250°C, with diameter equal to that of the shaft of the macor probe. A thin plate rectangular plate with a matching groove for the o-ring , and of equal dimensions of the rectangular pocket is used to press the o-ring and seal the probe cylindrical surface and hence preventing any leakage. The ALTP probe is held on its back by a phenolic sheet support. A braid shielded Coaxial cable connects the SMB connector on the ALTP probe to the final 50ft BNC cable that transmits the data to the acquisition chassis. All acquisition was done at 128KHz.

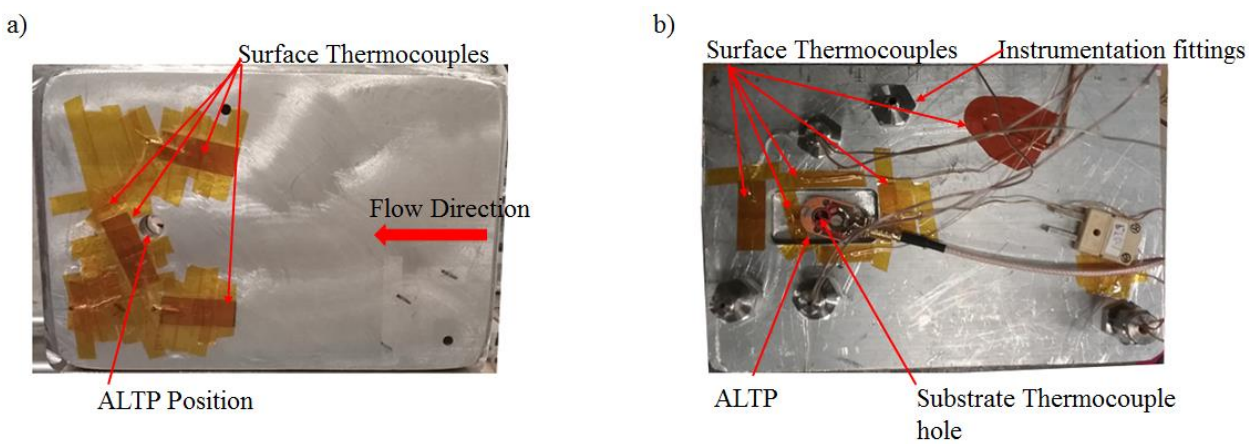

Figure 2.23 a) Flow exposed side of the instrumentation insert showing the location of the ALTP probe and surface thermocouples. b) Outside surface of the instrumentation insert showing the location of the rear surface thermocouples, the ALTP and the thermocouple for the substrate temperature.

As shown in Figure 2.23b) there is a hole at the back of the probe where another thermocouple is passed through to measure the temperature at the back of the film substrate and the hole is then

sealed with omega high temperature cement to prevent air from disturbing the result. The flow exposed surface of the insert form a part of the upper plate of the cuboidal test section.

The working principle of the experiment is that when flow is initiated, the thermocouples measure the change in wall temperature along with the change in temperature of the back of the film substrate and the insert. The temperature values from the flow exposed thermocouples and back substrate readings are inputted to a numerical code that computes the temperature profile inside the ALTP film and substrate based on input properties. For this case, we have used constant material properties despite the ALTP film being anisotropic. The code solves a one-dimensional heat transfer model of the film and substrate to give a temperature map varying with time based on the experimentally measured value. This temperature map is then used to compute the heat flux with time. The ALTP signal is compared to this calculated heat flux.

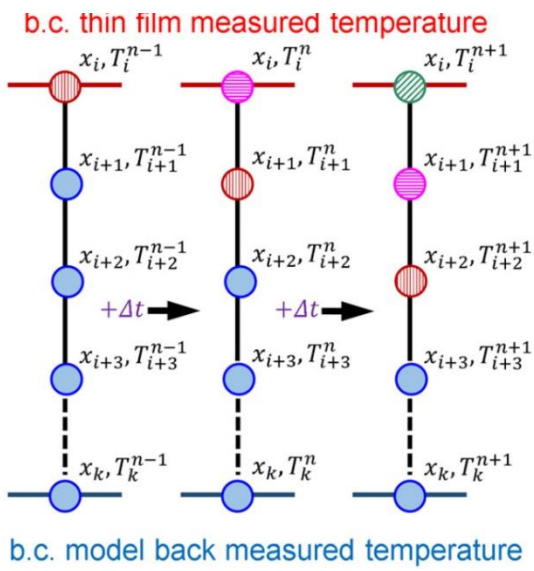

Figure 2.24 Graphical representation of the one-dimensional heat transfer code used for heat flux evaluation using thermocouples.

The numerical solver solves the 1D unsteady state heat conduction given in Equation (2.8) by using a Crank Nicholson numerical discretization.

$$\frac{1}{\alpha}\frac{\partial T}{\partial t} = \frac{\partial^2 T}{\partial x^2} \tag{2.8}$$

This discretization is first order scheme in space and second order in time and gives second order convergence. It combines both the forward Euler method for at n and the backward Euler method at n+1.

$$\frac{u_i^{n+1}-u_i^n}{\Delta t} = \frac{1}{2}\left[F_i^{n+1}\left(u,x,t,\frac{\partial u}{\partial x},\frac{\partial^2 u}{\partial x^2}\right) + F_i^n\left(u,x,t,\frac{\partial u}{\partial x},\frac{\partial^2 u}{\partial x^2}\right)\right] \tag{2.9}$$

The solver uses the measured wall temperatures as the boundary conditions and the heat flux continuity condition at the interface of the two layers.

$$-k_1\left[\frac{\partial T}{\partial x}\right]_{x=L-} = -k_2\left[\frac{\partial T}{\partial x}\right]_{x=L+} \tag{2.10}$$

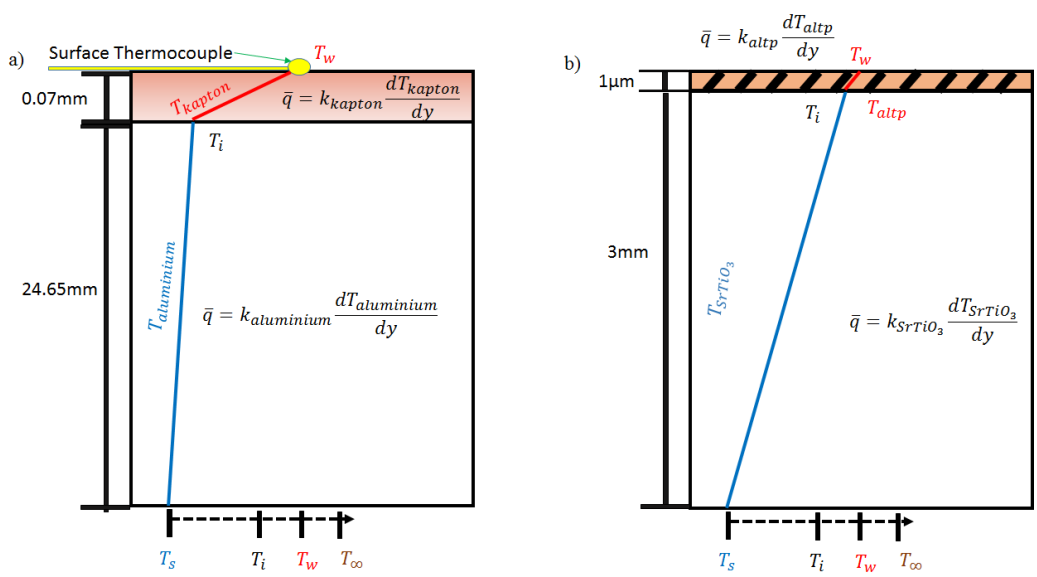

Figure 2.25 a)Schematic of the 1d heat transfer actually measured using surface thermocouples, b)Schematic of the heat transfer through the ALTP sensor.

2.5.2 Thermocouple Calibration

Since this methodology relies on the heat flux computed using surface thermocouples, the uncertainty associated with the surface thermocouples is of the utmost importance to reduce the total uncertainty in the calculated heat flux. A similar calibration technique used to calibrate RTD's is applied to the thermocouples. A Fluke constant temperature well was taken within which the thermocouples to be used were inserted. Eight fixed temperatures were used and the calibration was carried out five times to give in total of forty calibration points. The temperature of the well is compared with the readings taken by an ITS-90 compliant high accuracy Thermometer. A VTI EX1048A thermocouple measurement system was used to record the thermocouple output. The VTI system also records the temperature of the junction where the thermocouples are connected to the system using a series of high accuracy RTD's. This cold junction temperature is also recorded along with the raw voltage signal of each thermocouple. The thermocouple voltage is then compared to the temperature difference between the well temperature and the cold junction temperature. The thermocouples were kept at the well temperature for 30minutes, and the test window was taken when the cold junction temperature was constant. This does mean that window taken for different points and different runs were different depending on the cold junction temperature for that case. The average values of the voltage and the temperature difference were used for the calculation of temperature uncertainty.

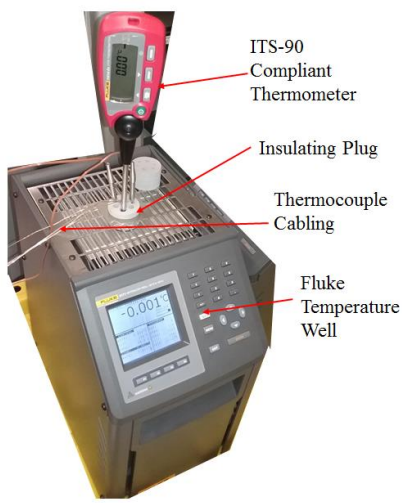

Figure 2.26 Arrangement of the Fluke Temperature Well and thermocouples during calibration.

It is assumed that the dependence of thermocouple voltage and temperature difference across its two junction is perfectly linear and hence follow the following equation

$$\Delta T = slope * V + intercept \tag{2.11}$$

The objective was to find the value of slope and intercept for each thermocouple and find the corresponding uncertainty in temperature measurement for a 95% confidence interval(CI). The R-squared value for the thermocouples were computed to check how accurate the assumption of perfect linearity holds. An average value of 0.99978 is found for all thermocouples with the values for the thermocouple used in one of the runs documented in table XX.

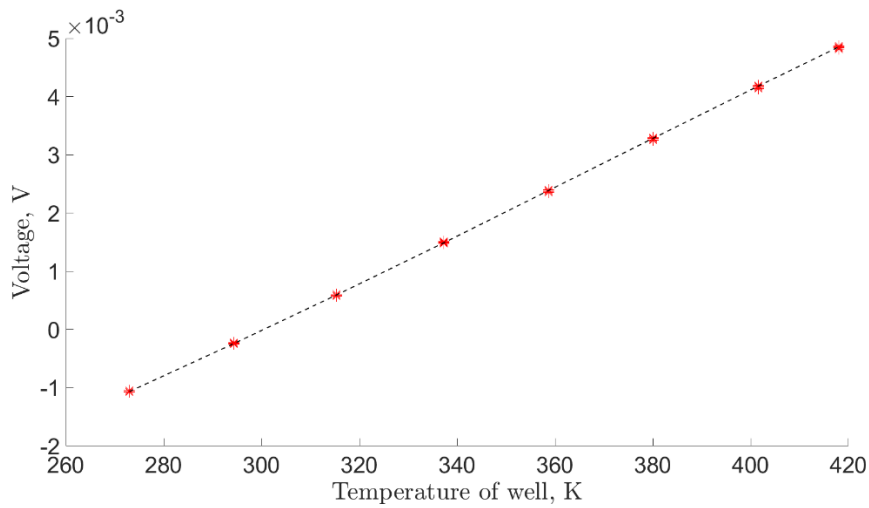

Figure 2.27 Calibration curve for one thermocouple showing linear trend between sensor voltage and temperature of the well.

Based on the work by Bornstein and Semendjajew[39], the uncertainty for the linear regression coefficients, namely slope and intercept are computed as below

$$|\ Slope\ uncertainty\ | < \frac{t_{\alpha,n-2} s_y \sqrt{1 - r_{xy}^2}}{s_x \sqrt{n-2}} \tag{2.12}$$

$$|\ Intercept\ uncertainty\ | < \frac{t_{\alpha,n-2} s_y \sqrt{1 - r_{xy}^2} \sqrt{\sum_{i=1}^{n} x^2}}{s_x \sqrt{n-2} \sqrt{n}} \tag{2.13}$$

where, $t_{\alpha,n-2} = Critical\ value\ for\ Student - t\ distribution$

$$s_y = Sample\ average\ square\ of\ deviations\ of\ \Delta T = \frac{\sum_{i=1}^{n}(y_i-\bar{y})^2}{n-1} \quad (2.14)$$

$$s_x = Sample\ average\ square\ of\ deviations\ of\ V = \frac{\sum_{i=1}^{n}(x_i-\bar{x})^2}{n-1} \quad (2.15)$$

$$r_{xy}^2 = Square\ of\ correlation = \frac{\sum_{i=1}^{n}(x_i-\bar{x})(y_i-\bar{y})}{\sqrt{\sum_{i=1}^{n}(x_i-\bar{x})^2\sum_{i=1}^{n}(y_i-\bar{y})^2}} \quad (2.16)$$

$$n = number\ of\ samples$$

The slope and intercept uncertainty is calculated for each thermocouple and then the calibration relative uncertainty for the temperature is calculated based on the sum of the squares of the individual uncertainty as the following-

$$\frac{\partial T}{T} = \sqrt{\left(\frac{Voltage * slope}{T}\right)^2\left(\left(\frac{\partial slope}{slope}\right)^2 + \left(\frac{\partial V}{V}\right)^2\right) + \left(\frac{Intercept}{T}\right)^2\left(\frac{\partial Intercept}{Intercept}\right)^2} \quad (2.17)$$

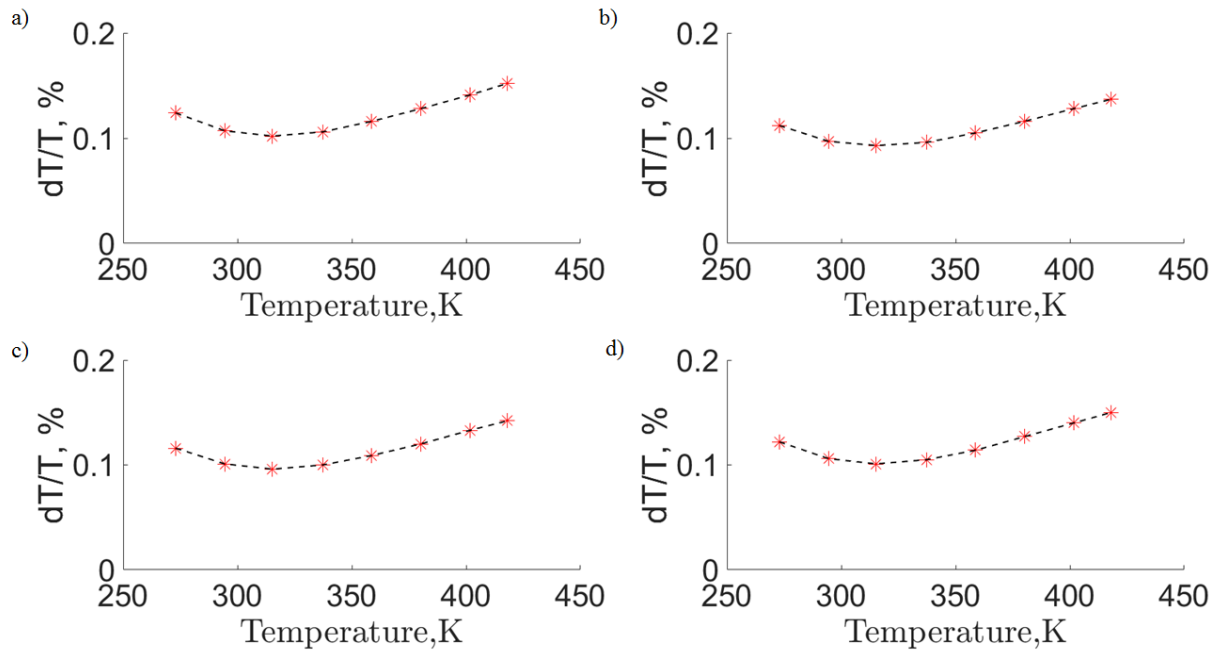

Figure 2.28 Relative Uncertainty in temperature plots for different thermocouples as a function of temperature.

This calibration methodology gives an average calibration uncertainty of around 0.14% at 400K, which translates to 0.56K.

2.5.3 Uncertainty Estimation

The uncertainty in the measurement of the heat flux using surface thermocouples relate to the uncertainty involved into the measurement of the parameters involved in the calculation of the heat flux using the numerical one-dimensional code. The code calculates the temperature distribution across the kapton tape over which the surface thermocouple is mounted and the aluminium insert. To estimate the effect of the uncertainty of each parameter, the heat flux calculation was done with the values of the uncertainty added for each parameter. The uncertainty value for each parameter was taken for a 95% confidence interval using measurement or literature. The uncertainty values for one heat flux point is shown in Table 2. The calculation is run with the maximum change in the mean value of the absolute uncertainty. Then the percentage of change of the calculate heat flux is compared to the percentage change of the mean value to compute the sensitivity of the heat flux calculation to that input parameter. To calculate the total uncertainty in heat flux, the

methodology of Moffat[3] was applied, where the root of the sum of squares of each percentage change in heat flux for each parameter is taken as the total uncertainty in the calculation of the final quantity. The uncertainty for the temperature was added as random errors for both the font wall temperature and the back wall temperature of the order of magnitude of the uncertainty in temperature measurement obtained from the calibration of the thermocouples. This was done to ensure that we don't introduce any bias errors in the calculation of the uncertainty, since for temperature measurement, a case of bias error essentially implies that the mean value of the heat flux will be different and if the bias is known, it can be compensated for.

From the table it can be seen that the code is very sensitive to the properties of the Kapton tape including the thickness. It is most sensitive to the temperature readings on both side of the wall and hence the need for accurate temperature measurement.

Table 2.2 Uncertainty table for heat flux value based on the Kapton and Aluminium layer.

	Mean Value	Units	Uncertainty	Sensitivity (%)
Kapton film Thickness	0.00007	m	0.00001	77.3
Aluminium Thickness	0.024765	m	0.00001	171.7
Kapton film Density	1420	Kg/m^3	0.71	145.0
Kapton film heat capacity	1090	J/KgK	10.9	15.0
Kapton Thermal Conductivity	0.12	W/mK	0.0036	79.7
Aluminium Density	2700	Kg/m^3	108	2.7
Aluminium Heat Capacity	897	J/KgK	27	0.9
Aluminium Thermal Conductivity	180	W/mK	7.2	13.6
Front Temperature	317.83	K	0.31783	549.4
Back Temperature	314.18	K	0.31418	549.4
Heat Flux Value	$9.51X10^3$	W/m^2	Total Uncertainty	11.30%

The average value of uncertainty through the numerical code is around 10-11% based on the 95% CI uncertainty values.

A similar study was carried out assuming that the temperature read on the flow exposed side is the same temperature on the surface of the ALTP film.

Table 2.3 Uncertainty table for heat flux based on the ALTP film and substrate system.

	Mean Value	Units	Uncertainty	Sensitivity (%)
ALTP film Thickness	0.000005	m	$3X10^{-6}$	0.7
Substrate Thickness	0.003	m	$1X10^{-5}$	95.7
ALTP film Density	6680	Kg/m^3	380	0.5
ALTP film heat capacity	374.25	J/KgK	0.94	6.5
ALTP Thermal Conductivity	2	W/mK	2	0.4
Substrate Density	5116	Kg/m^3	306	4.8
Substrate Heat Capacity	580	J/KgK	0.00696	0.01
Substrate Thermal Conductivity	12	W/mK	2	47.3
Front Temperature	304.5	K	0.3	2543.1
Back Temperature	298.8	K	0.3	
Heat Flux Value	$2.4X10^4$	W/m^2	Total Uncertainty	15%

The heat relative uncertainty value changes with the mean value of heat flux. From the list of sensitivity, it can be seen that the highest sensitivity of the code is with the temperature difference between the two measurement wall. The other major parameter effecting the heat flux is the thermal conductivity of the substrate material. Since the thickness of the ALTP film is extremely thin and the order of thermal conductivity of the film is close to that of the substrate material, the temperature distribution inside the system is a function of the thermal conductivity of the substrate, hence any errors in the determination of that value leads to a huge variation in the temperature distribution and hence the heat flux.

2.5.4 Results

Figure 2.29 shows the behavior of the temperature and the computed heat flux value as the valve is opened for a sudden discharge experiment. A sudden jump in the free stream temperature can be seen, as the ambient temperature inside is exposed to the hot flow and then the flow temperature can be seen to continue rising. This continuous rise in temperature is a result of the operation of the PETAL wind tunnel where the flow loses heat to the surrounding piping and the mass of the settling chamber and the test section as the temperature gradient is very high immediately after the

opening of the valve. The temperature stabilizes within 3-5 minutes of continuous flow, depending on the inlet conditions of the flow. The sudden jump in temperature is also registered by the wall mounted surface thermocouples, though the intensity is definitely much lower. The back of the substrate temperature changes relatively slowly as the heat flow takes time to dissipate to the positon of measurement. Figure 2.29b) shows the corresponding behavior of the ALTP voltage signal from the valve opening. The initial temperature jump provides the highest heat flux reading and is used for comparing the ALTP reading with the computed heat flux from the thermocouples. Figure 2.29b) showing the ALTP voltage behavior is filtered at 4Hz to better visualize the heat flux behavior, however the values taken for the calibration are from the raw signal. As can be seen that the noise fluctuations in the calculated heat flux signal is significantly higher than the fluctuations seen in the input temperature signal. However, these fluctuations seem to be comparable to the fluctuations seen in the ALTP voltage signal.

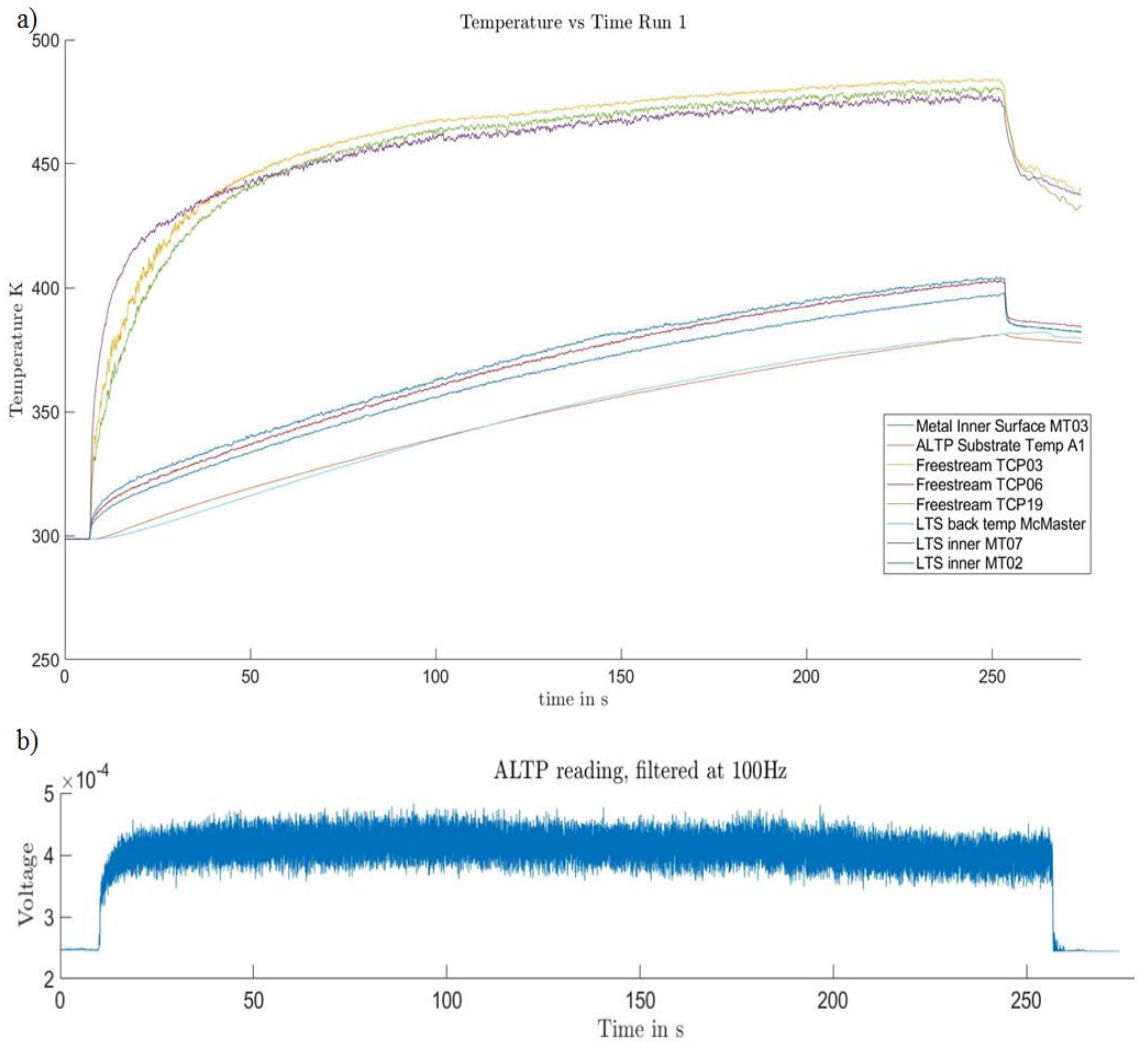

Figure 2.29 a)Temperature variation inside the test section on the opening of the valve, b)ALTP raw signal on the opening of the valve.

The major objective of this methodology was to obtain the calibration curve of the ALTP film showing the linear dependence of the voltage induced inside the crystal and the input heat flux. Figure 2.30 shows that dependence for different values of heat flux obtained during the different test runs for this method.

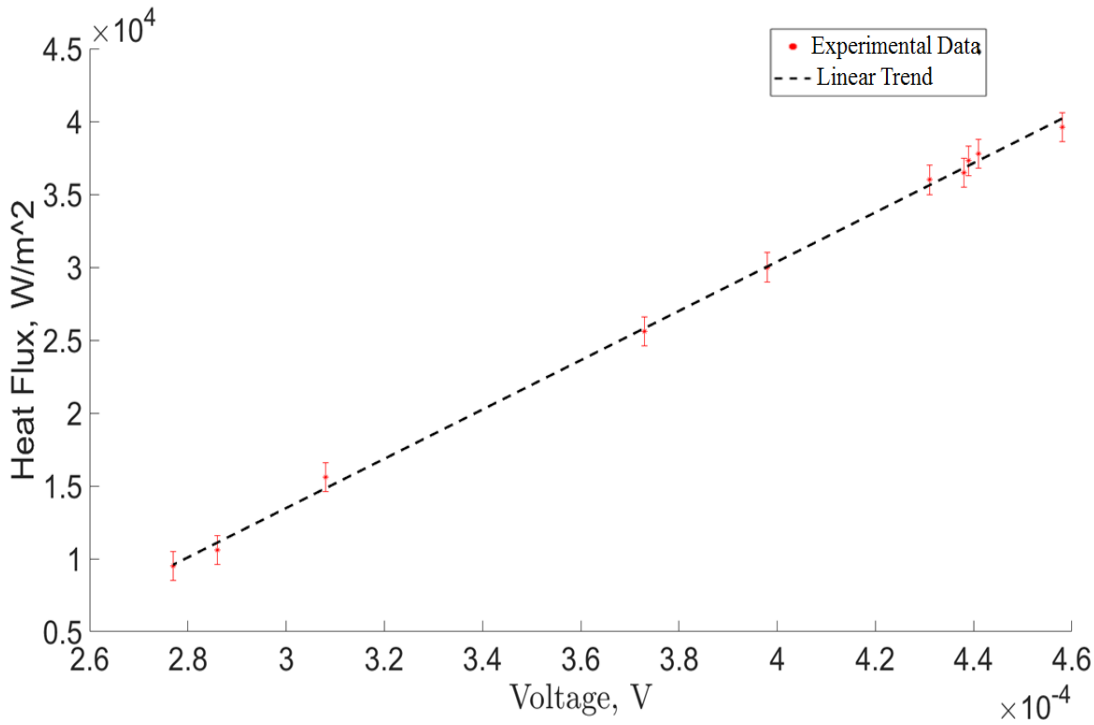

Figure 2.30 Calibration curve showing linear behavior between ALTP voltage and Heat Flux. The uncertainty bands are based on the uncertainty in prediction of Heat flux from the thermocouples.

Figure 2.30 shows the uncertainty band that is calculated for the heat flux based on the uncertainty that is present due to the numerical calculation of the heat flux. If the data is treated as a sample and its uncertainty is estimated through statistics, the bands are different. Since the points are very close to a linear trend the uncertainty estimates using linear regression is of the order of 2% but increases to 7% as we go lower in the value of heat flux as seen in Figure 2.31.

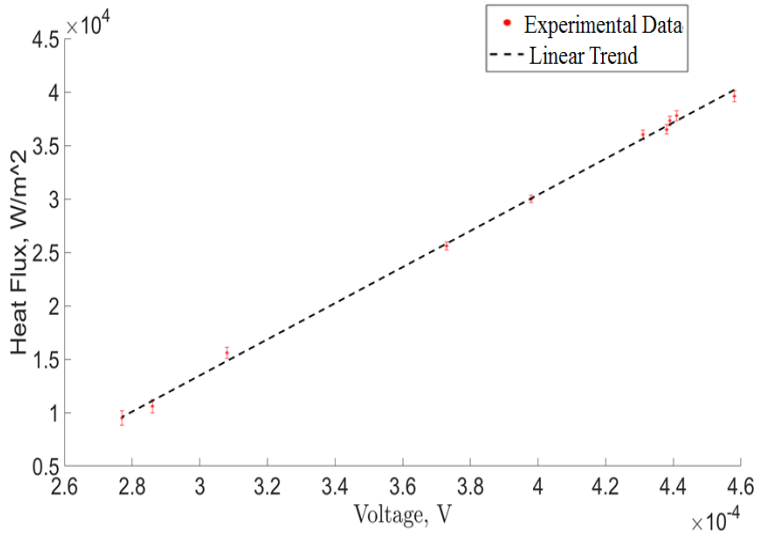

SSE=1.86X10 W/m^2

Estimated Standard deviation – 482.5W/m^2

Voltage,V	Heat Flux W/m^2	95 % Predicted Confidence Interval	% Change in predicted and measured
4.58E-04	3.96E+04	5.25E+02	1.3
4.41E-04	3.78E+04	4.61E+02	1.2
4.39E-04	3.73E+04	4.53E+02	1.2
4.38E-04	3.65E+04	4.50E+02	1.2
4.31E-04	3.60E+04	4.29E+02	1.2
3.98E-04	3.00E+04	3.58E+02	1.2
3.73E-04	2.56E+04	3.57E+02	1.4
3.08E-04	1.56E+04	5.37E+02	3.4
2.86E-04	1.06E+04	6.32E+02	6.0
2.77E-04	9.52E+03	6.73E+02	7.1

Figure 2.31 Calibration Curve showing the error bands based on 95% confidence prediction interval based on statistical inferences.

The correlation value for Figure 2.30 is 0.99926 with a R^2 value of 0.9985. Ten points were taken in total for sensor and the slope calculated as 169094082.3 V/ (W/m^2) with an intercept value of -37251. W/m^2, giving a sensitivity of 59µV/W/cm2. The default value of the ALTP stays around 2.3X10^{-4} for zero input heat flux. The uncertainty for each point is compiled in Figure 2.31 along with the error bars for the curve.

With the statistics of the ALTP response available, the mean values for its behavior was treated to the same analysis that was applied to compute the slope and intercept uncertainty for the thermocouple signal and hence compute the predicted uncertainty in the evaluation of heat flux based on the computed slope and intercept and a measured ALTP reading. The derivation is highlighted in section 1.5.2 and 1.3.3, giving the final dependence of the relative heat flux uncertainty as in Equation (2.18).

$$\frac{\partial Q}{Q} = \sqrt{\left(\frac{Voltage * slope}{Q}\right)^2 \left(\left(\frac{\partial slope}{slope}\right)^2 + \left(\frac{\partial V}{V}\right)^2\right) + \left(\frac{Intercept}{Q}\right)^2 \left(\frac{\partial Intercept}{Intercept}\right)^2} \quad (2.18)$$

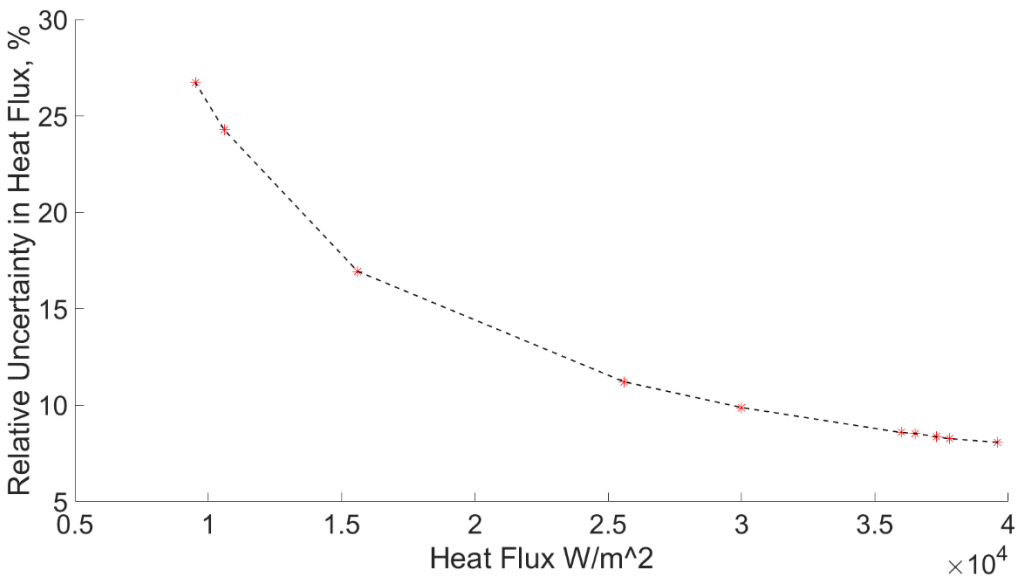

Figure 2.32 Relative Uncertainty for heat flux for ALTP calibration based on slope and intercept uncertainty.

As can be seen in Figure 2.32, the relative uncertainty follows a square root polynomial, with its minima at much higher value of heat flux than the conditions tested. For practical cases of interest, it can be seen that the relative uncertainty decreases with increasing value of input heat flux. However, for relatively low values of heat flux, upto 10Kw/m^2 typically found in wind tunnel testing, the relative uncertainty is near the standard 20% value. As expected, this method of predicted uncertainty gives a value much greater than the uncertainty estimated based on the heat flux calculation and incorporates sources of uncertainty that cannot be easily treated in the initial uncertainty estimates.

2.5.5 Limitations

Though, it gives a more desirable estimation of uncertainty, there are several limitations of this methodology. Firstly, it is still a secondary calibration technique, i.e. the sensor is still being compared to another sensor that can give greater accuracy in the mean value. It is not comparing against a primary source of calibration. This implies that this method suffers from the inaccuracy related to the sensor it is being calibrated against with, namely wall mounted surface thermocouple. Also in this methodology, the heat flux is not being directly measured, but rather it is being calculated based on the readings from a secondary sensor. This is one of the primary reasons for

the relatively high uncertainty associated with this methodology. Since the calculations of the heat flux are very sensitive to input parameters of the ALTP film system and the thermal properties of the sensor system are difficult to measure accurately and to take into effect the temperature of operation has on its readings, it is very difficult to eliminate the uncertainty that is inherent to the heat flux calculation. The calculation is also based on a numerical approximation and not on an exact solution. This, while allowing the simplification of an otherwise complex system of equations whose solution without approximation does not exists yet, also induces the uncertainty that is inherent to the numerical approximation and is sensitive to the spatial grid and the temporal resolution of the input temperature readings. From the methodology point of view, the appropriate temporal resolution requirement translates to the requirement of fast sampling of the temperature to ensure that the heat flux gradient is captured with sufficient accuracy. This not only imposes a condition on the data system used, but it also opens up another source of uncertainty namely, that of different response time of the ALTP film and the sensor it is being calibrated against. The ALTP can operate in the order of 100 KHz, while the response of the thermocouples is of the order of 200-300 Hz at maximum [40]. For sudden change in flow conditions, the response of the ALTP signal will be different to the response of the thermocouples, and this makes the selection of the window to compare the heat flux and the ALTP voltage even more challenging. Another source of uncertainty is the heating of the thermocouples by the flow. Ideally since the thermocouples are in contact with the metal insert, they should read the temperature on the metal surface. However, one side of the thermocouples are exposed to the flow, and despite there being present a thermal barrier between the junction and the flow, the flow will act as a heat source or sink, depending on the flow conditions, and that will affect the readings of the temperature from the thermocouples. The methodology also banks on the assumption that the temperature of the flow exposed metal wall is the same as the temperature of the flow exposed ALTP film. This is not going to be true since we know that the wall temperature of the boundary layer of a flow is greatly affected by the type of wall and how much heat it can conduct away from the wall. Though this methodology tries to calibrate in such a way so as to eliminate the effect on the wall heat flux of the presence of the sensor, there will be distortion in the wall heat flux due to the presence of the sensor and its compensation is not easy since there is no accurate way to measure the temperature on the wall of the ALTP film.

CHAPTER 3. HEAT FLUX MEASUREMENT IN HIGH SPEED SHOCK WAVE ENVIRONMENT

3.1 Review

Heat flux is an important parameter for high speed flow applications such as hypersonic flights and supersonic combustors. It is extremely important for flows where the aerodynamic heating over the surface becomes dominant in the total heat distribution over the surface. There are also fluctuations in free stream or fluctuations caused by interaction of moving shock waves with boundary layer that maybe be at a faster frequency than the sensors used are capable of resolving. Gardon type gauges and thermocouples have been used as the mainstay for temperature and heat flux measurement. Lin[40] utilized Gardon gauges for the thermal measurement in a supersonic nozzle. The work of Cook [41] advanced the data reduction technique for application of thin film gages to shock tubes, bringing this temperature measurement methodology to the realm of supersonic testing. While these sensors are effective at measuring the mean value of the heat flux, they are in general insufficient in measuring high speed fluctuations in the heat flux which is common occurrence in high speed phenomenon. Beresh[44] showed that how pressure fluctuations measured in supersonic and hypersonic boundary layers were dependent on the resolution of the senor and historically the database has been biased low. This highlights the need for faster instrumentation to better understand the supersonic boundary layer. Specially designed coaxial thermocouples have been used by Menezes[42] to measure wall temperature in a hypersonic tunnel with a response of a few microseconds. Thin films have been used by Owen[43] to measure the transition of supersonic boundary layers by looking at the RMS values of the fluctuation across the test article, with higher RMS values of the boundary layer in the turbulent section. Even the ALTP has been shown to be effectively utilized to measure heat flux variation of second mode instability waves found in hypersonic boundary layers in the works of Kegerise[22]. All of these works highlight the importance of high speed measurement for the supersonic regime and the need for faster instrumentation to better characterize the boundary layer.

3.2 Experimental Methodology and test conditions

To measure the heat flux under conditions of sudden changes in heat flux, it was decided to see the sensor performance under supersonic conditions. It is expected that the sensor will be exposed to sudden shocks which will be equivalent to pulse change in heat flux and the it should be able to measure the boundary layer oscillation in the presence of strong shock and the transition of the flow from supersonic to subsonic as the wind tunnel is unstarted. To achieve this, a supersonic test section was required. The linear wind tunnel at PETAL located at Zucrow labs, has the flexibility of condition of both upstream and downstream pressure to generate supersonic flow inside its test section. A supersonic nozzle was used with the area ratio of 1.6875 of the exit to the throat area to give a maximum of Mach 2 at the exit of the nozzle. The sensor was installed in the diverging section of the nozzle in the hopes of picking up the shocks during the unstarting of the wind tunnel. The nozzle was designed to generate supersonic flow for another test article placed downstream of the nozzle and is discussed in the works of Braun[2].

As shown in Figure 3.1 the nozzle begins at the starting of the test section, chokes the flow at the throat, and then expands it to supersonic conditions. The insert system of installing instrumentation discussed in 1.5.1 is again utilized at the top wall of the linear test section to provide access to the required instrumentation inside the wind tunnel. The insert containing the ALTP is based on the same setup as discussed in 1.5.1 and is still instrumented with surface thermocouples to compare with the readings of the ALTP and contrast the fluctuations in the thermal boundary layer picked up the surface thermocouples and the ALTP.

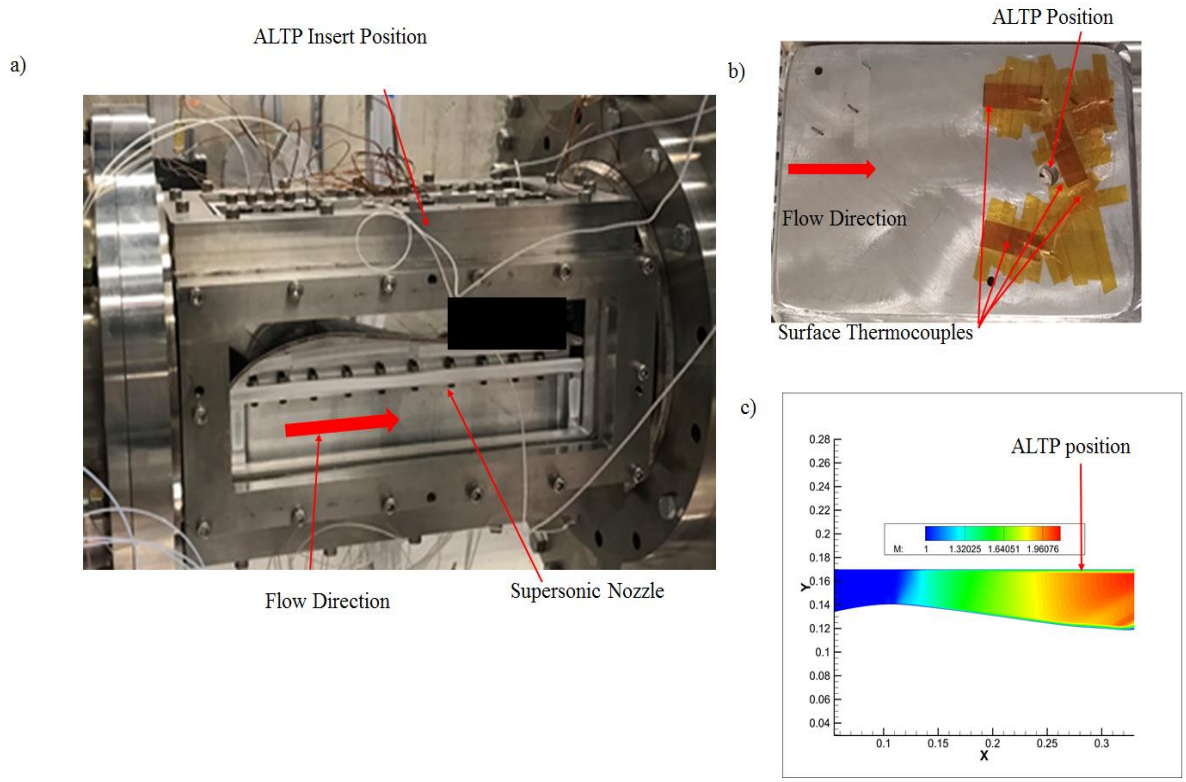

Figure 3.1 a)Supersonic flow test nozzle b)Flow exposed surface of test insert used for ALTP c)Numerical Mach contours of the nozzle showing the Mach number at the ALTP location.

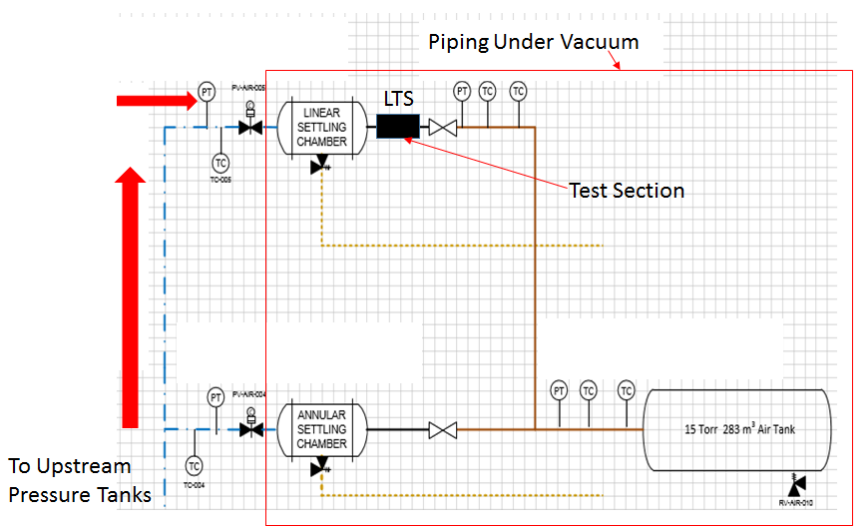

Figure 3.2 Piping Diagram showing the piping under vacuum for supersonic flow.

To achieve supersonic flow, the entire wind tunnel and all the piping from the linear wind tunnel fast actuating valve to the vacuum tank, as marked in Figure 3.2 was kept in vacuum. The vacuum

was pulled using a pump through a dedicated exit line in the piping and was kept continuously running for the entire duration of the test. The system was run in vacuum to reduce the total pressure requirement to achieve Mach 2. At Mach 2, for isentropic flow, the static to total pressure ratio is 0.1278. So if the wind tunnel was operated at atmospheric pressure, 1.01325 bar, then the total pressure requirement would have been 7.9 bar, which is much higher than the rating of the piping upstream. This high pressure also restricts the total duration of the testing. The pressure inside the wind tunnel was dropped to 100milibars to achieve supersonic conditions. The length of the test was restricted by the total volume of the vacuum tank and the subsequent rise in pressure. The nozzle maximum pressure of operation was 0.129 bars for atmospheric pressure upstream. With a higher back pressure, shocks will start to develop in the nozzle and the wind tunnel will get unstarted. The length of testing depends on the mass flow being tested. On an average every run would last for around 120 seconds. Multiple runs were carried out spread over multiple test days and in between runs, the vacuum pump was kept running to allow to reach lower pressures to increase the duration of the test run. This was important for conditions with hot flow to achieve near stable conditions in terms of the temperature of the flow. As discussed in the 1.5.4, due to the operational procedures of the linear wind tunnel, since the flow loses heat initially to the surroundings once the fast response valves are opened, the temperature for hot flow conditions continue to rise before attaining steady state conditions. For vacuum operation, achieving steady state temperature becomes more difficult due to very short test runs.

Both cold flow and hot flow conditions were tested. The cold condition was compared to the CFD analysis done by Braun[2] for the supersonic nozzle and the attached test article.

3.3 Experimental Uncertainty

The primary source of measured uncertainty was the uncertainty in the calibration used to map the ALTP signal to heat flux. Another source of uncertainty maybe incorrect installation or leakage inside the test article from the various instrumentation holes and the edges of the test section walls and the insert walls. This small leaks could affect the flow inside giving a different value of the heat flux than what will be expected for the set flow conditions. Also an improper fitting of the insert with the test section wall, the presence of instrumentation, like the curvature of the

thermocouples, in supersonic flow, act as a source of shock generation, which will greatly affect the wall heat flux.

For the heat flux evaluated using surface thermocouples, as discussed in 1.5.3, the uncertainty depends on the uncertainty of the input parameter to the heat flux code, which include the thermal properties of the ALTP film and substrate and also the input measured temperature. An additional source of error for the surface thermocouples, is that the effect of the flow as a temperature source or sink, distorting the temperature reading, becomes more pronounced in supersonic flow due to the high speed of the flow increases the total heat transfer.

3.4 Results and Discussion

Multiple runs of different temperature and constant mass flow were carried out and the readings are presented in the following. It is seen that the ALTP reading match well with the readings from the surface thermocouple, though the standard deviation around the mean value for the ALTP film is much higher than for the surface thermocouple.

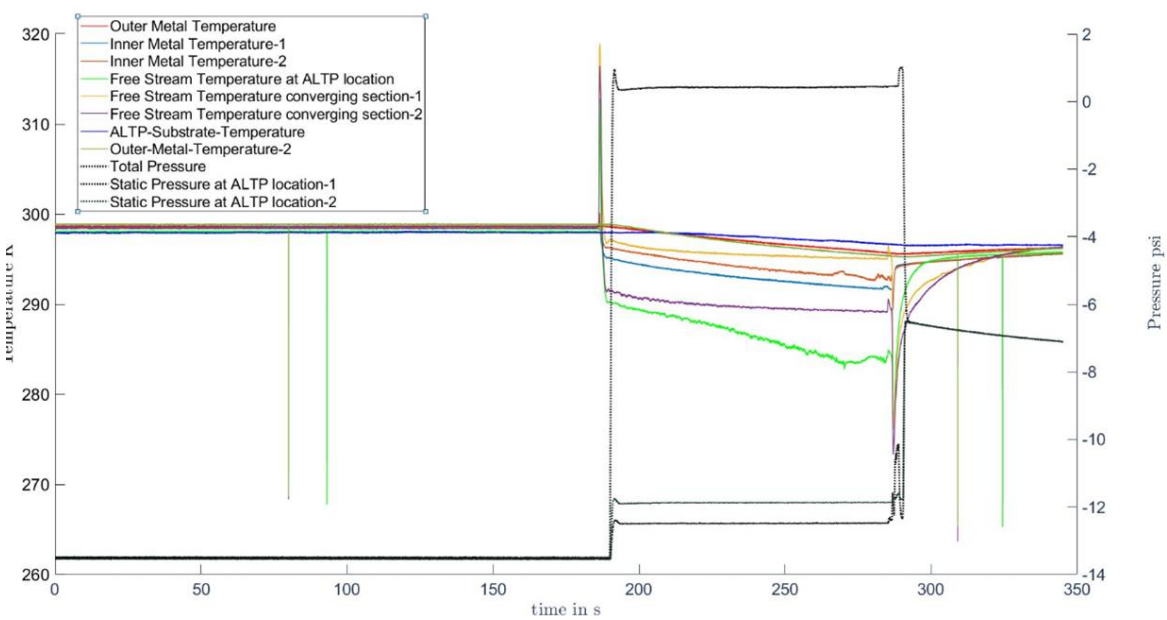

Figure 3.3 Temperature and Pressure behavior inside the test section during one run with the supersonic nozzle with hot flow.

Figure3.3 shows the temperature and pressure readings for a typical run. In this case the flow is supersonic throughout the test duration, as can be seen with the constant pressure ratio between the total and static pressure. The flow condition is cold and hence a temperature drop is seen for all of the thermocouples. The thermocouple measuring freestream temperature at the ALTP location has massive velocity errors due to it being in supersonic flow and hence it is much colder than the thermocouple present in the converging section of the nozzle. Thermocouple-2 in the converging section slipped in its clamp and was touching the metal surface of the nozzle and hence its temperature was different from the other free stream thermocouples. The back of the substrate temperature measured for the ALTP is inside a cavity inside the probe body with no free convection, hence it stays hotter than the thermocouples exposed to the back of the insert, since the back of the insert is directly exposed to ambient air.

Figure 3.4c) shows the heat flux for the same run as Figure 3.3 As can be seen, the trends on both the ALTP and the surface thermocouple match very closely. The maximum heat flux reached is $1.5X10^4 W/m^2$ in the region where the free stream temperature reaches as stable value of 287K.

Figure 3.4 shows the test results for each of the separate runs for the supersonic nozzle. Fig 3.4b) has the flow changing from supersonic to subsonic due to increase of the back pressure beyond the maximum pressure required to choke the nozzle. Figure 3.4c) shows the steady and dropping heat flux value for which the heat transfer coefficient was attempted to be calculated. For all cases it can be seen that the ALTP is much more sensitive to flow fluctuations and gives a more oscillating signal. It is also able to pick up the shock waves at the beginning of the test much better than the surface thermocouple. In Figure 3.4b) we see the ALTP pick up separation in the diverging nozzle when the flow regime changes from supersonic to subsonic.

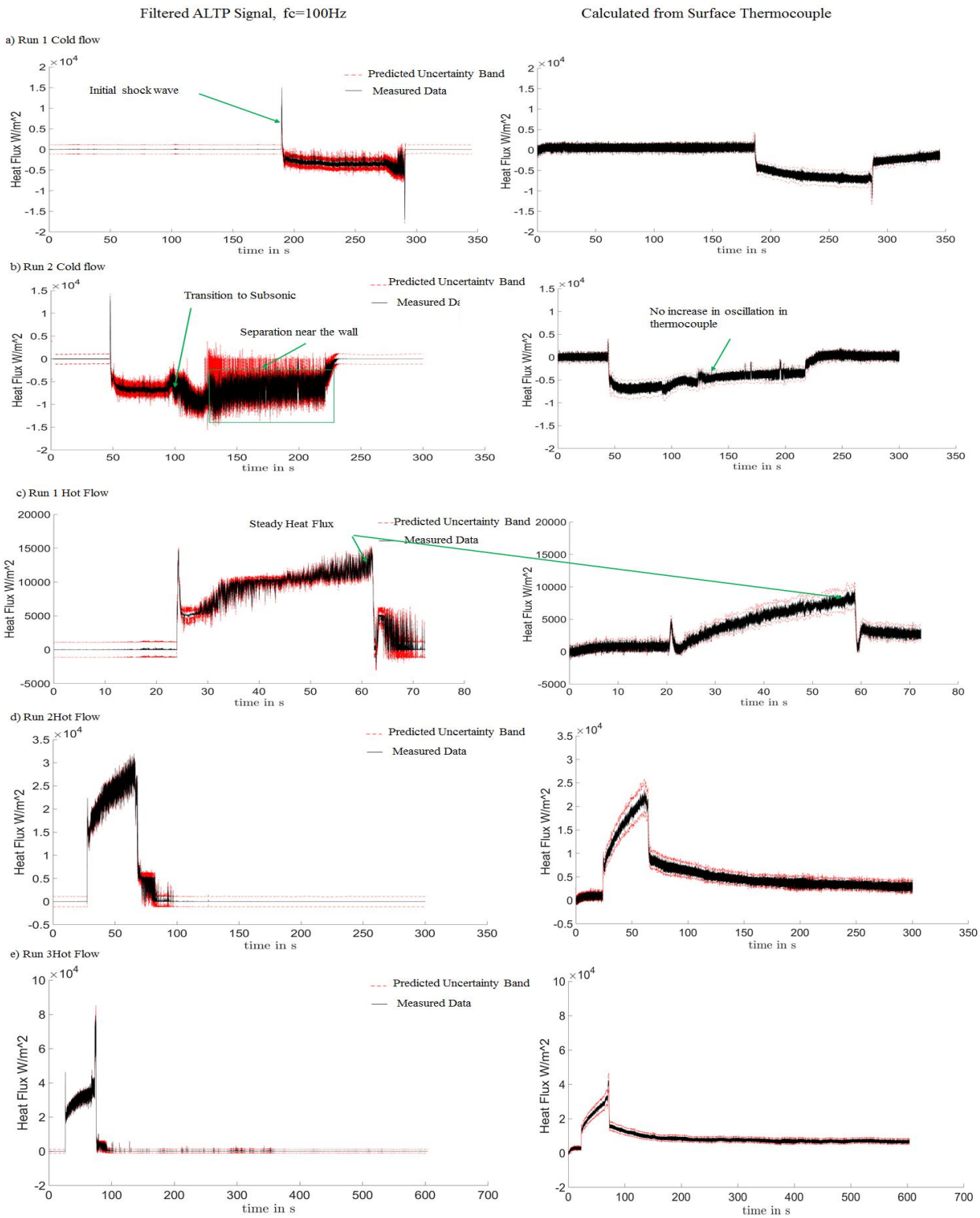

Figure 3.4 The first column shows ALTP heat flux reading for different test runs and column two shows the surface thermocouple derived heat flux.

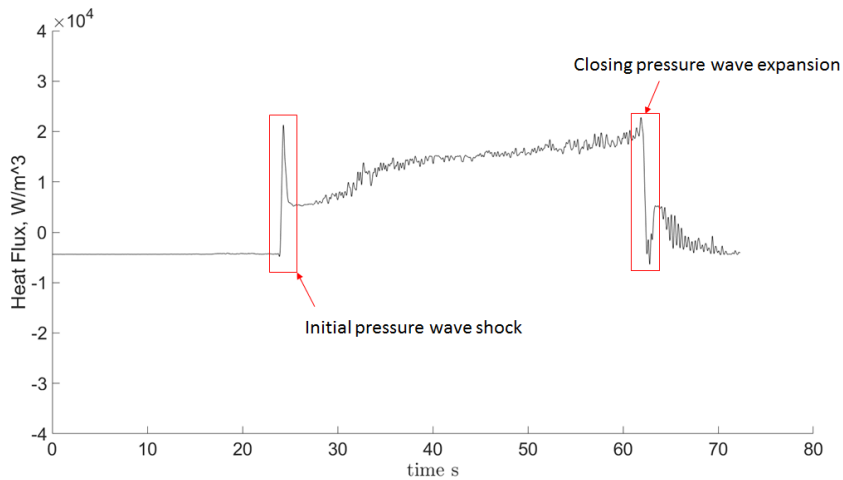

Figure 3.5 ALTP signal for Run1 Hot flow at 4Hz to show sharp changes in heat flux during shock and expansion wave inside wind tunnel.

Figure 3.5 shows the filtered value of the ALTP reading for the same run to better visualize the flow features and the presence of the initial shock as the nozzle is started. These peaks in temperature are present in even for subsonic flow due to the pressure wave generated as the valve is opened. However, the intensity of these wave is greatly amplified as the wave is accelerated to supersonic in the nozzle and the effect of the starting of the nozzle, where a shock is passed from the throat to the exit of the nozzle.

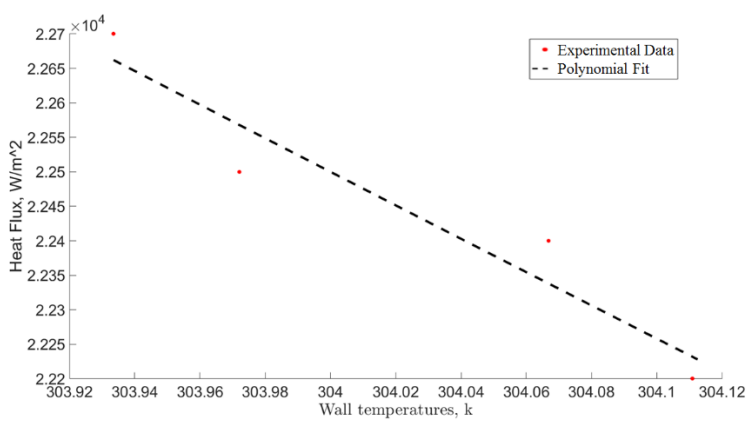

Figure 3.6 Decrease of heat flux with increasing wall temperature for constant flow temperature.

Achieving steady state temperature for hot flow conditions is difficult for vacuum conditions due to the short window of testing, however we did achieve near steady temperature in the free stream for one of the runs. Here the heat flux starts to decrease as the wall temperature increases. This trend is shown in Figure 3.6. Based on the work of Lavagonoli[4] the heat flux is related exponentially with the adiabatic wall temperature and the temperature difference as

$$q = h_{ad} * \left(\frac{T_w}{T_{ad}}\right)^n (T_{ad} - T_w) \tag{3.1}$$

Based on the definition of the adiabatic wall temperature as the temperature where the wall heat flux is zero, the trend seen in Fig 3.6 is extrapolated to give and adiabatic wall temperature of 315.25K with a heat transfer coefficient using Equation (3.1) as 2465W/m^{2}K.

CHAPTER 4. DESIGN OF COOLING SYSTEM FOR COMBUSTOR HEAT FLUX MEASUREMENT

4.1 Review of Heat Flux measurement in combustors

Heat flux measurement inside combustors is a challenging prospect due to the high heat loads and high operational temperatures present. The ALTP itself has been used in a similar environment in SI engines in the work of Lejsek[21], but the duration of exposure was short enough that it did not warrant active cooling of the system. Thermocouples are ideal for combustors since they can survive high temperatures, especially coupled with a suction probe, these suction pyrometers have been widely used for heat flux estimation as evident by the works of Hanby [34] and Watanabe[35]. Thermocouples without suction probe have also been used such as the work of Marshall [36]. Optical Pyrometers and Liquid crystal measurement (Ireland [37]) for heat transfer are also common methodologies for combustors with optical access.

However, there is a lack of very high speed temperature measurement inside combustors for engines to industrial units. Since thermocouples the most commonly used sensors for combustors can go upto a few hundreds of KHz, and for the conditions inside combustors. Also, generally the wires used are thicker and more resilient to withstand the extreme conditions, this leads to a further decrease in the maximum frequency of the measurement. For slow systems such as industrial furnaces, this will not matter much, but for systems with very fast changes in heat flux, such as internal combustion engines or detonation tubes, fast response temperature sensors are required. Since not every such system will have optical access to be able to use pyrometers, a sensor such as the ALTP is ideal since it is fast and can be recessed in the walls of the combustor with little distortion to the flow inside. However, the conditions found inside most combustors are much more extreme than the ALTP can withstand. Therefore, a cooling system is required for long testing durations.

4.2 Review of cooling strategies applied to probes for high temperature

For testing of systems that operate under very high temperatures, the cooling of instrumentation is the only way to ensure their survival. Plasma systems operate at temperatures of thousands of

Kelvin and the inside of Gas Turbine combustors can have free stream temperatures of upto 2000K. There aren't a lot of materials that will survive such harsh conditions, hence cooling is important. However, cooling systems come with their own issues and problems. The cooling systems need to be compact enough so that they minimize the distortion to the system that will occur due to the inclusion of a cooled probe. A pitot tube or a total temperature probe are placed in the flow path, hence they distort the flow which they are trying to measure. A very thick probe will distort it further. For wall mounted sensors, a cooling system will change the temperature distribution around the sensor and change the effective wall property to be measured, either wall shear or heat flux. Numerical methods have made design of components much easier, and using conjugate CFD, it is easy to optimize cooling systems. Brouckaert et al [40] designed a cooled total pressure probe using a water cooled jacket and they optimized the design using two dimensional axisymmetric analyses before they moved to full three-dimensional analysis.

4.3 Description of the ALTP cooling problem

To allow for continuous measurement in high temperature environments such as inside a combustor or in the first stage of a high pressure turbine, it is imperative that the sensor is maintained at its maximum operational temperature to ensure both that the film survives and that the heat flux readings are not distorted much due to the change in the properties of the film and substrate with temperature. The maximum continuous operational temperature of the ALTP film is quoted as 50°C or 323K. This value is a conservative estimate given by the fabricators of the film and the system is able to survive and operate at much higher temperatures, a fact that was inadvertently proven in one of the calibration test discussed in 1.5.4 where the exposure time was long enough that the substrate temperature reached near 140°C. However, as a design point, the value of 323K was taken with a tolerance of 5K around the design point for steady state operation. Since the sensor is wall mounted, a simple geometry of a flat plate was chosen and a typical heat transfer coefficient of 2000W/mK calculated for a free stream temperature of 1273 K was taken for the maximum convective heat load that the film has to survive. This implies that a cooling system was needed that could effectively maintain a drop of 950K across a film of 5-micron thickness. Other constraints on the design are that the total volume of the sensor and the cooling

system was to be kept as small as possible to ensure minimum disturbance of the test section by the introduction of different materials and active cooling of the surface.

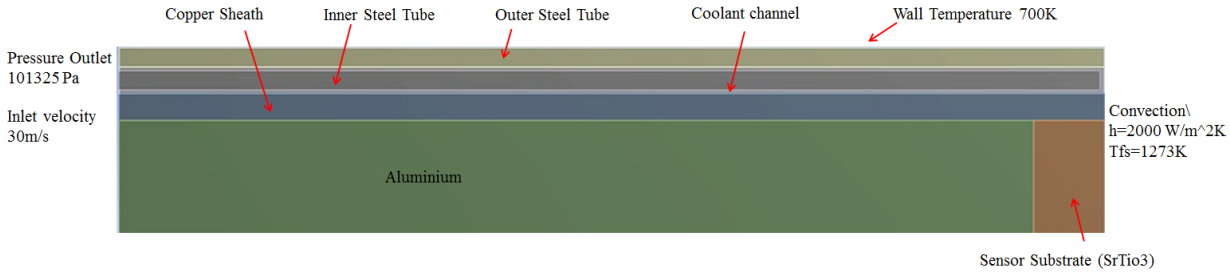

Figure 4.1 Basic schematic Geometry of the ALTP cooling system.

Figure 4.1 shows the basic schematic layout of what such a system might entail. Taking the same dimensions of the sensor that are discussed in this work so far, we replace the macor casing around the sensor probe with the cooling system. The idea behind the system was to achieve the target temperature at the interface of the sensor substrate and the film since due to the very small thickness of the film, we can neglect the temperature drop across the film. The initial idea is to use sensible cooling using a coolant circulated under pressure kept at low temperatures to act as a sink for the incoming heat load. Sensible cooling system is preferred since it is much easier to predict the flow in terms of computational cost and hence much faster to optimize than a system involving latent heat cooling due to phase change. It also simplifies the pumping system requirements and the broadens the scope of use of much easily available coolant. Since the sensor system will be mounted in wall of the test article, another source of heat load will be the temperature of the wall itself, which as a design point it has been taken as 700K based on the works of [] []. So the coolant should be able to take away the input convective heat load and heat load due to the gradient in temperature between the coolant and the surrounding wall of the probe. Also to protect the sensor substrate and aluminum body from coming in direct contact with the coolant and risking of contamination of the ALTP film and the electrical connections, a sheath or cover is needed to protect the probe body while at the same time this cover should add the least amount of thermal resistance between the substrate-film interface heat source and the coolant sink. Since due to the low conductivity of the substrate material, high temperature gradient will be present along the axial length of the probe, this cover should be able to take the heat from the substrate and spread it more evenly along its length to provide more effective heat transfer to the coolant. With these

considerations in mind, the design of an effective cooling system was approached first using a one-dimensional approximation to provide starting value of input parameters of the coolant, wall materials and geometry and then optimization using two-dimensional axisymmetric CFD.

4.4 1D Model

4.4.1 Model Description

As a first approximation a one-dimensional model was conceived between the various components of the cooled probe system. The system was broken in to block and assigned material properties. The driving temperature were the average temperature of each block and the thermal resistance between each system was taken to be the thermal resistance for a cylindrical system were the temperature variation is only a function of the radius. The heat flow model is shown in Figure 4.2. By taking the radius of the casing, r3, as the input parameter and relating all radius to r3, we are able to evaluate the cooling system for different values of r3. The heat input is assumed to be concentrated on the first block of aluminum shown as Q1, though Q1 is calculated based on the area of the entire probe and hence is itself a function of r3. Another major approximation done is that it is assumed that the temperature of the coolant after it passes through the coolant channel, shown as Tws is the same as the film substrate interface temperature. So for the coolant channels, both input and output, the heat has two parallel pathways, one to continue on from one block to the next, or to be absorbed by the flow and lead to a change in temperature of the coolant. The coolant used in this model is water and its properties are assumed to be constant with temperature. The intermediate walls forming the cooling channel were assumed to be made of acrylonitrile butadiene styrene (ABS) and the casing material was assumed to be copper. The first block behind the substrate was taken as Aluminum based on the available probe design where there is a backing aluminum stem on to which the substrate is fixed onto. The inlet temperature of the water was taken as 294K and based on different values of r3, the value of Water temperature at sensor, Tws and water temperature at outlet, Twout , were evaluated.

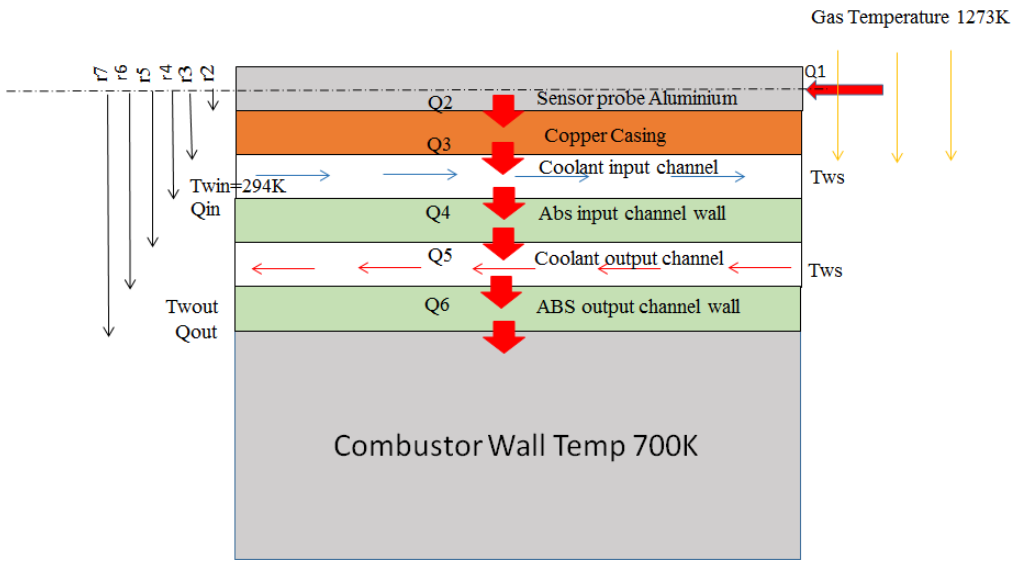

Figure 4.2 Block Diagram of the 1D model.

The Dittus-Boelter relation [7] for flow in pipes was used to estimate the heat transfer coefficient for the coolant in both input and output channel. On applying the conservation of heat for a steady state system the following system of equations were obtained that were solved in this model.

$T_{freestream}$ is taken as 1273K and T_{film} as 323K.

$$Q_1 = h_{gas}\pi r_6^2 (T_{freestream} - T_{film}) \tag{4.1}$$

$$Q_2 = \frac{\pi L(T_1 - T_2)}{\frac{\log\left(\frac{r_2}{r_1}\right)}{2K_{12}}} \tag{4.2}$$

$$Q_1 = Q2 = Q3 \tag{4.3}$$

$$T_{in} = \frac{T_{win} + T_{ws}}{2} \tag{4.4}$$

$$T_{out} = \frac{T_{wout} + T_{ws}}{2} \tag{4.5}$$

$$Q_4 = \frac{\pi L(T_{out} - T_{wall})}{\frac{1}{2h_4 r_4} + \frac{1}{2h_5 r_5} + \frac{\log\left(\frac{r_5}{r_4}\right)}{2K_{45}}} \tag{4.6}$$

$$Q_6 = \frac{\pi L(T_{in} - T_{out})}{\frac{1}{2h_6 r_6} + \frac{\log\left(\frac{r_7}{r_6}\right)}{2K_{67}}} \tag{4.7}$$

$$T_{ws} = T_{win} + \frac{Q_2 - Q_4}{mC} \tag{4.8}$$

$$T_{wout} = T_{ws} + \frac{Q_4 - Q_6}{mC} \tag{4.9}$$

$$r_5 = r_4 + 0.5X10^{-3}\ (m) \tag{4.10}$$

$$r_7 = r_6 + 0.5X10^{-3}\ (m) \tag{4.11}$$

$$0.0023\, Re_d^{\frac{4}{5}} * Pr^{0.3} = \frac{hd}{k}\ [7] \tag{4.12}$$

$$m = \rho\pi(r_4^2 - r_3^2)v \tag{4.13}$$

Where ,

$m = mass\ flow\ of\ coolant$

$C = Heat\ Capacity\ of\ coolant$

$K = Thermal\ Conductivity\ of\ block$

$r = radius\ of\ block$

$T = Temperature\ of\ block$

$h = heat\ trasnfer\ coefficient\ of\ block\ and\ coolant\ at\ wall$

$Q = heat\ flow$

$L = Length\ of\ Block$

$Re = Reynold's\ Number\ of\ coolant$

$Pr = Prandtl\ Number\ of\ coolant$

$\rho = Density\ of\ coolant$

$v = Inlet\ velocity\ of\ coolant$

Based on the model we obtain maps of the temperature of the outlet water temperature, T_{wout}, the water temperature at the sensor, T_{ws} and the wall temperature of the outer wall in contact with the coolant, T_6 with changing radius r_3 and inlet velocity of coolant.

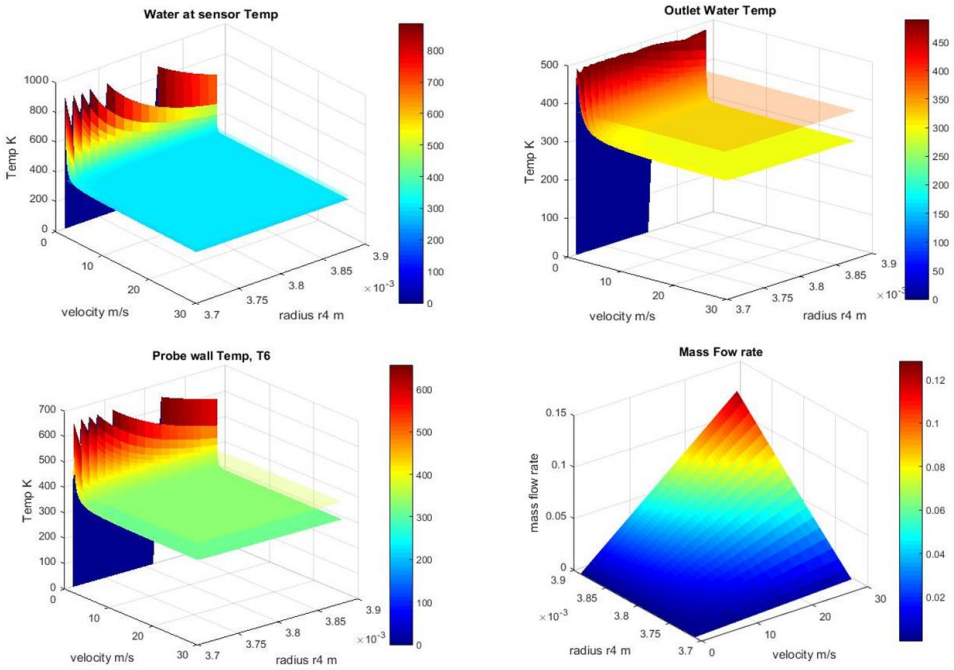

Figure 4.3 Contours of the quantities of interest from the 1D code, the water at temperature sensor , the outlet water temperature, the probe wall temperature and the mass flow rate as a function of the velocity and the parameterized radius.

4.4.2 Limitations

The model predictions give us a starting point for the design parameters, however the biggest limitation of this approach for this cooling problem is that the model deals with average values of temperature. It is effective at predicting average values, but as will be seen in 3.5.4, there are very high temperature gradients present in the system, especially in the region of interest, namely the substrate, due to the insulating nature of the substrate thermal conductivity. So even if the average temperature is below the design point temperature, the temperature at the substrate-film interface can be much higher. The model cannot also take into account the local heating of the coolant near the walls on the outlet channel. Since the dimensions of the cooling channel is very small, this restricts the amount of mixing in the flow and essentially dampens out most of the inlet turbulence. This means that the very hot coolant near the walls doesn't get mixed with the much cooler coolant

in the centre of the flow and hence there is a chance of localized boiling along the wall. This phenomenon cannot be captured through the one-dimensional approach and thus any values obtained from this approach must be verified against at least a two- dimensional analysis which can capture such gradients. This model does however allow us to check the limits where the bulk average quantities of the different blocks will exceed the design limits and we can completely ignore those areas for the two-dimensional design.

4.5 2D axisymmetric numerical simulation

4.5.1 Geometry Description

The initial two-dimensional geometry is based on the schematic discussed in 3.4.1. It consists of a cover around the primary probe body which consists of the substrate and the aluminum stem. This cover is taken to be made of copper due to its very high thermal conductivity. The reasoning being that copper should be able to take the heat from the substrate and spread it out more evenly so that the heat is picked up by the coolant more effectively. The coolant passage is formed by the copper sheath and two tubes. The material of the tubes was taken as steel because based on the results from the one-dimensional model we can see that ABS with its low thermal conductivity is not able to drop the temperature across its length below its maximum operating point. Though ABS works well as a barrier layer for the coolant to ensure that the coolant will not heat up and allows the flexibility of being able to be printed in any shape using 3-D printing, the temperatures are too high and the material will melt. Steel is chosen due to its relatively low thermal conductivity compared to other metals and its ubiquitousness.

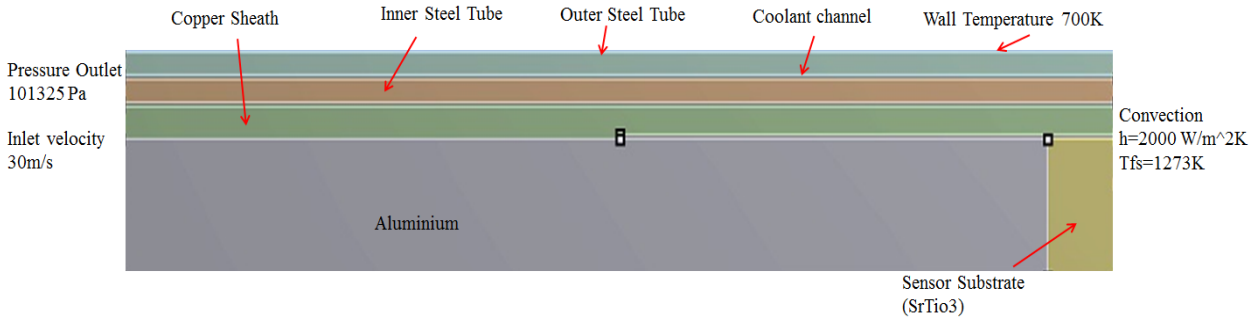

Figure 4.4 Schematic of the basic geometry used for 2D axisymmetric study.

A cap of around 1mm forms the bend of the coolant channel to allow the flow to go from the inlet to the outlet channel. This bend is necessary to route the flow and it has to be kept of sufficient thickness since this is the part of the structure that will take the brunt of the pressure of the coolant. However, the presence of this cap also reduces the total area covered by the coolant of the copper sheath and hence adds thermal resistance to the heat source at the substrate-film interface and the coolant heat sink. So the entire design process becomes to be able to increase heat transfer at the intersection of the inlet channel and the cap since that is the smallest path between the heat source and sink. Based on the results of this analysis the chosen geometry undergoes several iterations with new features being added to enhance this heat transfer and also material change to allow for better insulation from the surrounding wall and better structural resistance.

To increase heat transfer from near the flow exposed wall to the coolant sink, a material with more thermal conductivity than copper was looked into. Pyrolytic Graphite has very high thermal conductivity in the a-b plane of the sheet and low thermal conductivity along the c-axis. Copper has a thermal conductivity of 401W/mk, whereas a 100-micron thick sheet of commercially available graphite sheet boasts a 700 W/mk in the a-b plane. Thinner sheets have higher thermal conductivities. So a notch was added that was filled with a 100-micron thickness sheet with the intention that this sheet will better direct the heat from the substrate film interface to the rest of the cooling system. This layer also adds as an insulator for heat load coming from the cap to the substrate due to its very low thermal conductivity in the c axis. The effect of this layer is evaluated in 3.5.4

4.5.2 Boundary Conditions

As shown in Figure 4.4, the two-dimensional analysis was carried out on an axisymmetric geometry, with the axis being the centerline of the primary probe, i.e. the aluminum stem and the substrate. The inlet coolant was kept at an inlet velocity of 30m/s. This value was revised to 40 and then to 45m/s. The initial coolant temperature was kept at 294K, once it was found that this will be insufficient to cool the system, the coolant was revised to ethylene glycol-water mixture in the volume ratio of 60-40%. This mixture can be cooled to -42°C or 231K. The inlet temperature was set to -233K. The outlet of the coolant channel is assumed to be opened to atmosphere. The higher pressure of operation does imply that the boiling point and the freezing point of the coolant

will be different, but as design points, the boiling point and freezing point of the mixture was taken at 1atm, or 101325 Pa. As discussed in 3.3, the wall temperature is kept at 700K and the walls exposed to the flow have convection at a constant heat transfer coefficient of 2000W/mK at a free stream temperature of 1273K.

The analysis was carried out in Ansys Fluent, which is a finite volume solver. The solver type used is called the pressure based solver which belongs to a class of solver following the projection method. These class of solvers obtain the constraint of conservation of mass by solving a coupled pressure equation derived from the continuity and momentum equation to provide corrections for the velocity field [8]. This is commonly used for solving incompressible fluid, though it is capable of solving compressible fluids too at subsonic conditions. A conjugate analysis was carried out with all flow equations and the energy equation being solved for the coolant and just the energy equation being solved for the solid part of the domain. The discretization system used is second order upwind for all quantities. The criteria for convergence is the drop of all absolute residuals to a level of 10^{-6} below the last iteration and the matching of mass flow at the inlet and outlet, along with the stability of wall shear stress and total surface heat flux at each of the wall interfaces between the coolant and the solid.

4.5.3 Mesh Sensitivity

The domain was discretized using an unstructured mesh generator. The domain was populated with quadrilateral mesh with the face length kept as the mesh parameter. An inflation layer was added to the coolant with a y+ value of 0.1. The edges of the mesh of the solid and fluids on the interface walls were joined on a one is one basis, i.e. the mesh mapped to each other were in contact with each other as shown in Figure 4.5. A mesh sensitivity was carried out by changing the mesh parameter but the y+ for each mesh was kept constant. There were at least 15 points inside the boundary layer.

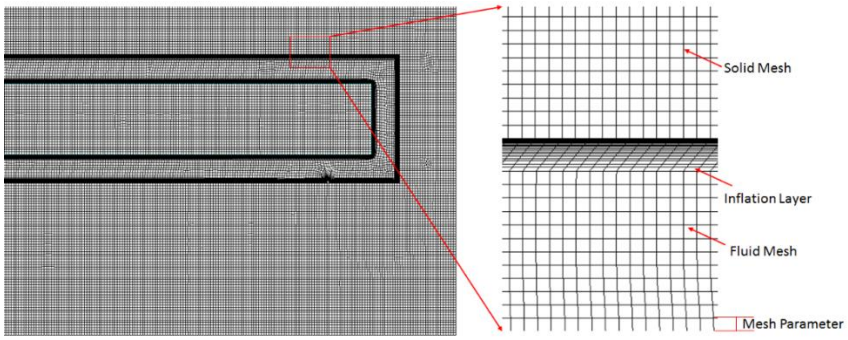

Figure 4.5 Mesh used for the 2D axisymmetric analysis with zoom in of the inflation layer and the conjugate solid-fluid interface.

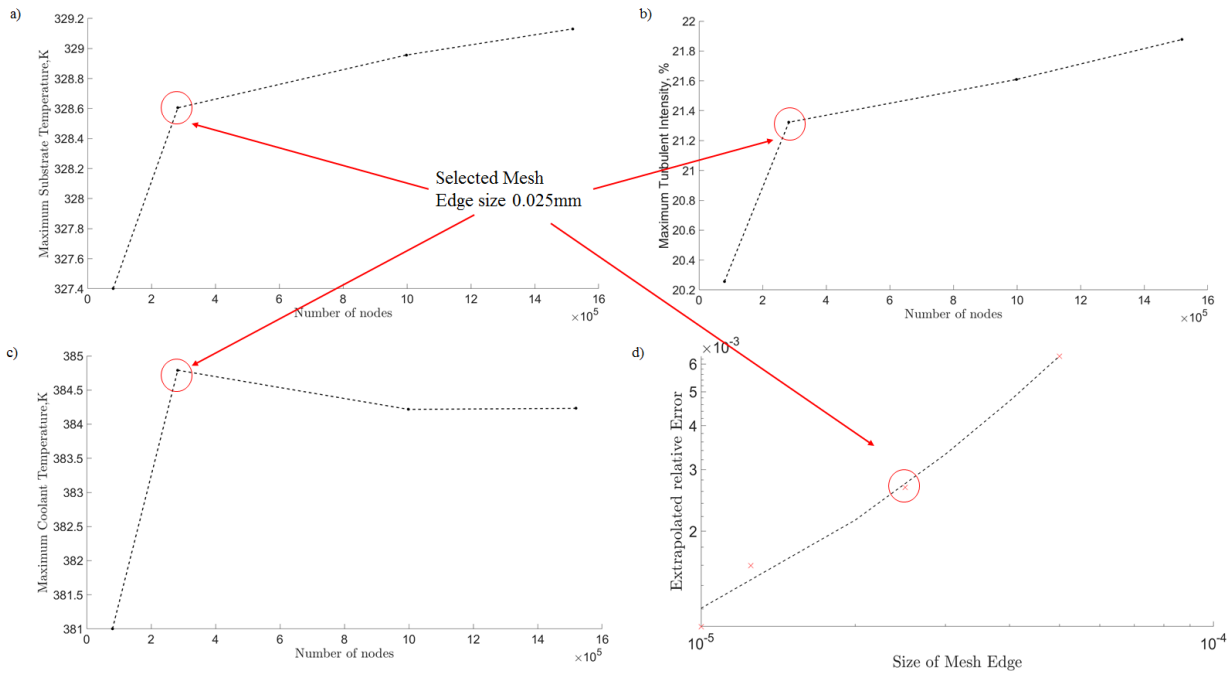

Figure 4.6 Mesh sensitivity results for the quantities of interest, a)The behavior of the Maximum substrate temperature with number of nodes, b)the trend of the Maximum turbulent intensity of the flow with number of nodes, c)The maximum coolant temperature with number of nodes, d) The extrapolated relative error for the maximum substrate temperature based on Celik[38] definition.

Figure 4.6 shows the mesh sensitivity results on quantities of interest in the domain namely the maximum temperature at the substrate film interface, the maximum temperature of the coolant and the maximum turbulent intensity of the flow. As can be seen that the values of the quantities have only variation of 0.14% for coolant temperature, 0.1% for the substrate temperature and 1.3% for

turbulent intensity, from mesh 2 to mesh 3, it was decided to use mesh 2 with 282741 nodes and a mesh parameter value of 0.025mm, to save on computational time.

4.5.4 CFD Results and Discussion

For the initial geometry and boundary conditions, we first evaluate the effect of the pyrolytic graphite sheet (PGS). Figure 4.7 shows the temperature contour and the area averaged heat flux along the walls for the substrate with copper and with PGS on the side of the substrate. All other boundary conditions being the same, it was found that the presence of PGS on the side enhances the heat transfer significantly and leads to a drop of 32K in the peak temperature of the substrate. It enhances the total heat transfer from the side of the substrate by 12% just due to its higher thermal conductivity. The PGS layer on the interface of the substrate and film wall was later abandoned as it was found it was possible to achieve target temperature without the cooling system extending to the front of the substrate.

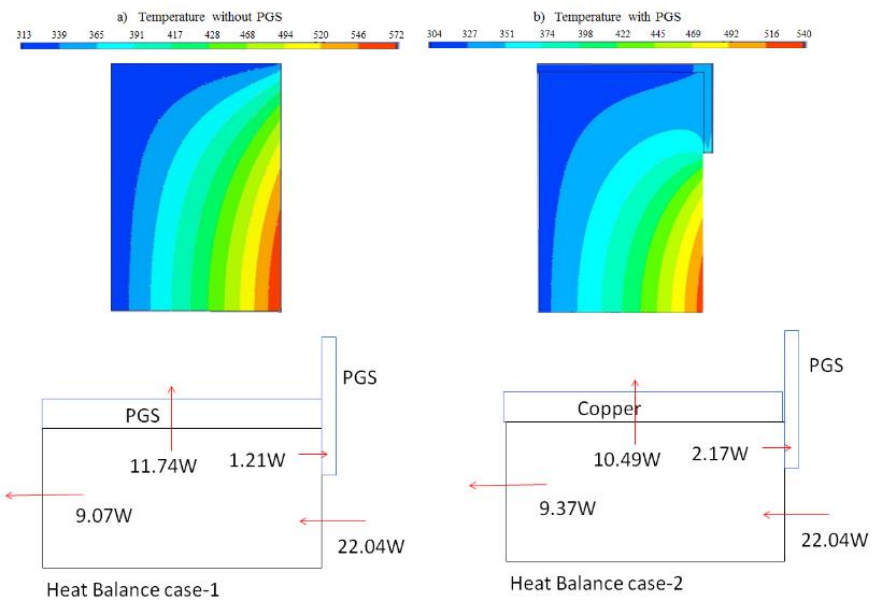

Figure 4.7 Temperature contour of substrate a) with PGS and showing the relative distribution of heat, b) without PGS and showing the relative distribution of heat.

One evaluation that was done before working further on the cooling design was to look into what will be the minimum temperature that will be needed on the substrate wall for the design heat flux input to achieve the required temperature at the film. This allowed to evaluate the effect of the

thermal properties of the substrate alone. Only the substrate was modelled with the film interface exposed to convective heat flux and every other wall kept at isothermal conditions. The low thermal conductivity of the Strontium Titanate substrate kept from achieving the design temperature till the isothermal wall temperature was set at 185K, lower than the boiling point of oxygen.

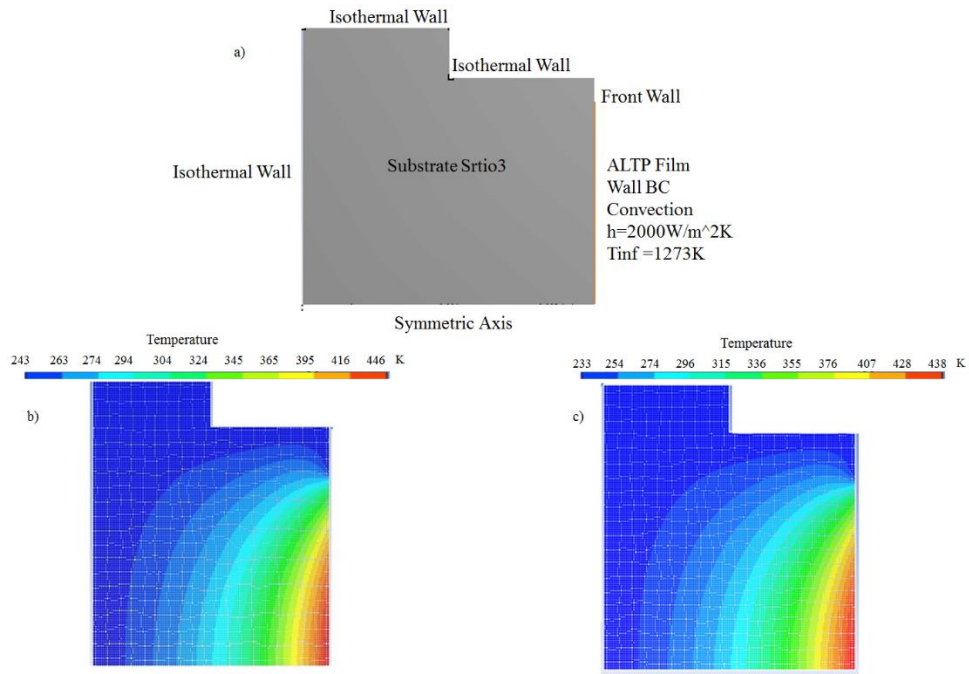

Figure 4.8 a) Geometry of the substrate analysis, b) Temperature contour of the substrate at 243K isothermal wall, c)Temperature of the substrate at 233K isothermal wall.

This result brings up a major hurdle. There was no effective way of cooling the film for the present configuration unless the system was dropped to cryogenic temperatures. This will be a very expensive solution, so alternatives were thought about. The simplest solution was to change the material of the substrate to something that has higher thermal conductivity. After discussions with the Dr Betz, of Fortech GmbH who makes the ALTP films, another substrate which was commonly used and readily available for depositing of the YBCO films was found, namely Magnesium Oxide, which has a thermal conductivity 4.5 times that of Strontium Titanate.

So for a cooled ALTP sensor capable of handling the temperature conditions commonly found in combustors for long duration tests, it was necessary to change the substrate material. For the same

evaluation of Magnesium Oxide as substrate, it was found that the temperature required is 278K. Based on this result the initial geometry was reinvestigated such that it was capable of generating a heat sink that was equivalent to an isothermal wall around the substrate kept at 278K.

To further enhance heat transfer near the bend of the inlet channel, a trip geometry was added to generate greater turbulence in the flow path as shown in Figure 4.9. The geometry chosen was a right angle triangle of 0.1 mm base and height based on the works of [], where a triangle was found to be very effective than other shapes.

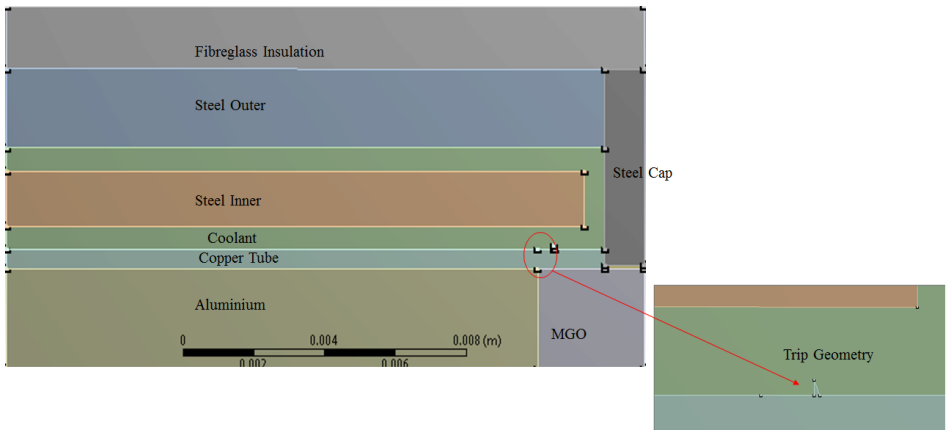

Figure 4.9 Revised geometry for 2D analysis using Magnesium Oxide and trip geometry.

With the introduction of this geometry and by increasing the inlet velocity to 45m/s, it was possible to achieve 328K at the substrate-film interface. There was further scope of improvement of the performance which was achieved by changing the shape of the coolant channel by adding a bend in the geometry of the copper sheath which follows the velocity streamline. The material of the jacket was again changed now to Inconel, which has even lower thermal conductivity than steel, but which is possible to 3D print, giving the final geometry as shown in Figure 4.10

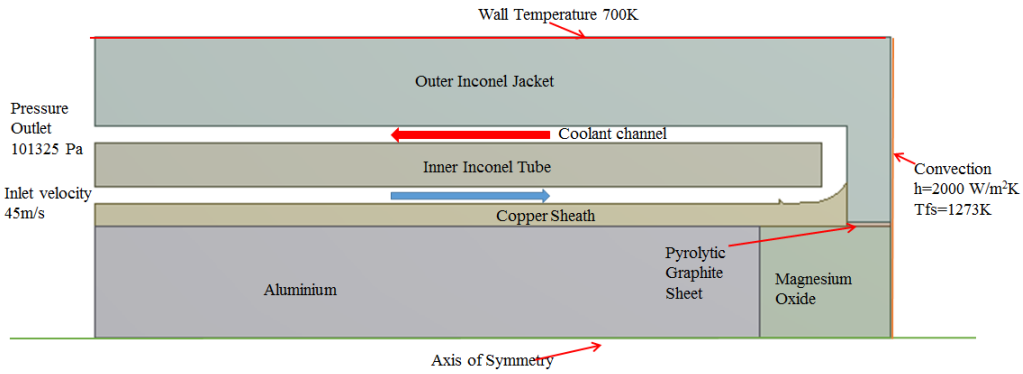

Figure 4.10 Revised Geometry with curved channel to further enhance heat transfer by preventing separation near the wall.

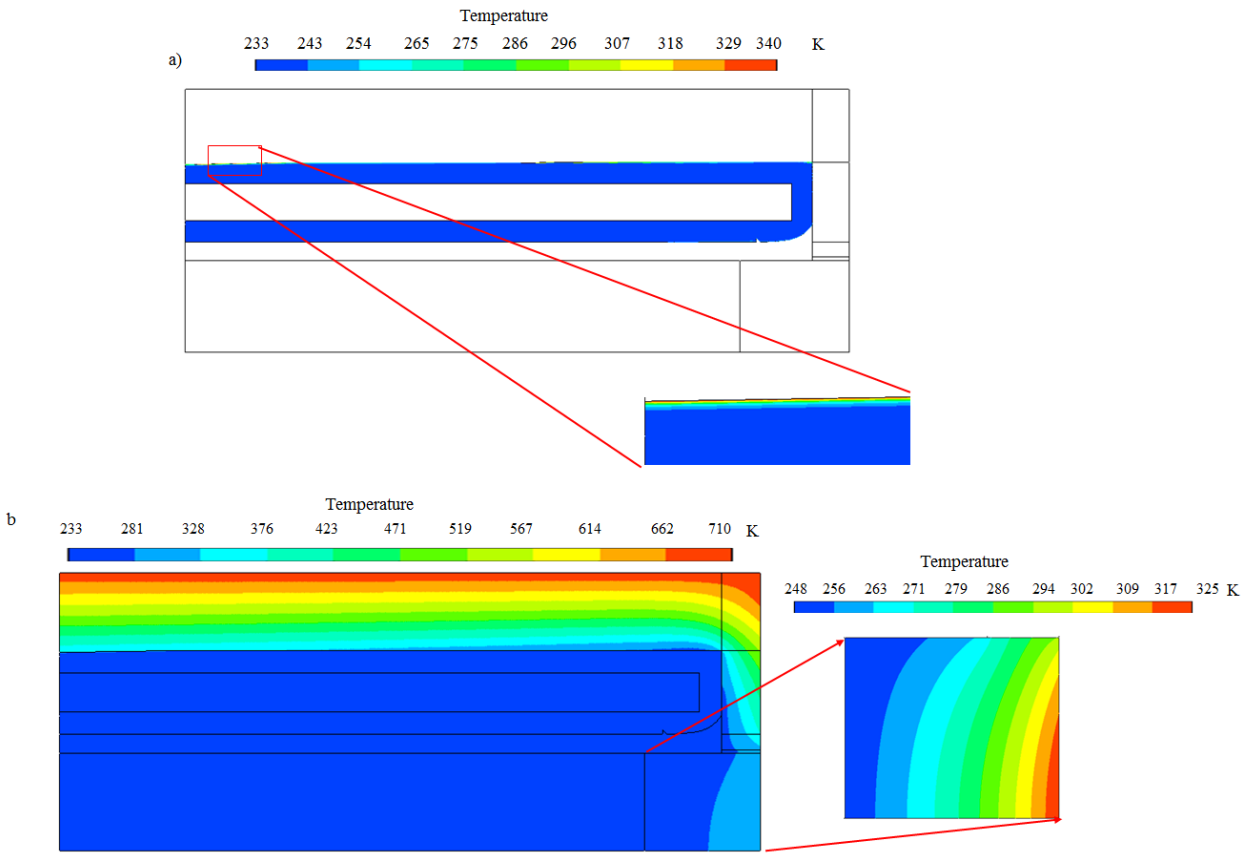

Figure 4.11 a) Temperature contour of the coolant showing the maximum temperature below the boiling point of the coolant, b) Temperature contour of the entire system showing the peak temperature on the outer wall and the zoom in of the substrate temperature contour.

The results of the evaluation of this geometry is compiled in Figure 4.11. The maximum coolant temperature had dropped from 371K using steel as the jacket material to 339K with Inconel due

to lower temperature of the coolant jacket wall interface. The maximum film temperature changed slightly from 325.3K to 324.8K with Inconel. The maximum temperature of the Inconel is 710K, well within its maximum operational temperature. The drawback of this system is though the high pressure requirement at the inlet to provide the required mass flow to provide sufficient cooling. For an inlet velocity of 45m/s, the input total pressure requirement is 45.9 bar.

4.6 2D axisymmetric Structural Analysis

4.6.1 Geometry Description

The solution from the CFD show that it possible to meet the design requirement within its tolerance by the present cooling system. However, since due to its very large pressure requirements, it is important to check whether this system will be able to hold the structural strain that the cooling system will generate and how much deflection and distortion will occur during operation. For this a two-dimensional axisymmetric static structural analysis was carried out to estimate the total deformation and to get an estimate of the total stress generated inside the probe. The geometry taken is the same with the boundary conditions shown in Figure 4.12. This analysis does not take into account time varying loads and fatigue analysis.

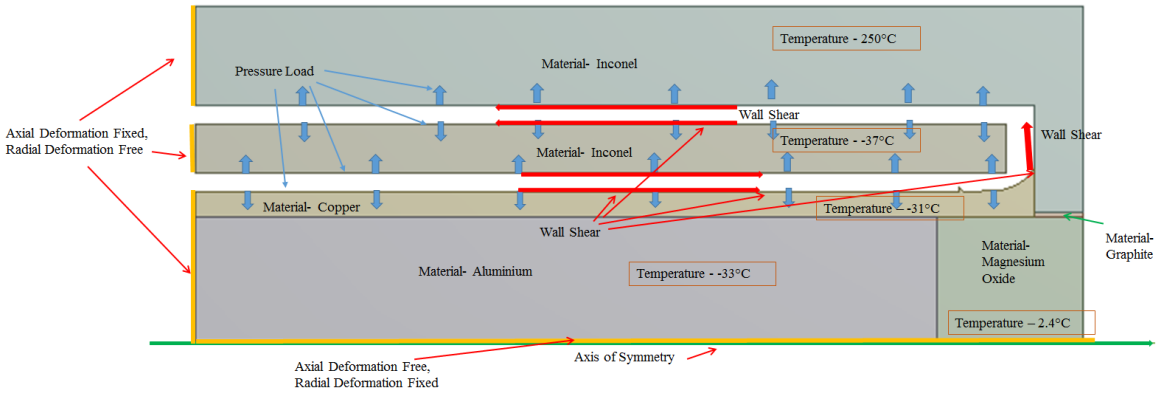

Figure 4.12 Basic Geometry and Boundary Conditions for the structural analysis.

4.6.2 Boundary Conditions

Each interface wall with the coolant has the area averaged pressure imposed on it that is calculated from the CFD. For the inner tube of the channel, each wall is exposed to a different pressure. Along

with the pressure, each wall is also exposed to wall shear in both the radial and axial direction, depending on the geometry. The material properties were taken from different sources and are temperature varying. Another condition that was imposed was the area averaged temperature for each material block. This was done to include the effect the temperature gradient present will have on the total deformation and the stress generated. The axis of geometry is the same as in the CFD. The support provided as shown in Figure 4.12, are free axial displacement but zero radial displacement along the axis. The leftmost wall is fixed in its axial displacement but free to move in the radial direction.

4.6.3 Mesh Description

The domain was discretized using an unstructured mesh generator. The domain was populated with quadrilateral mesh with the face length kept as the mesh parameter. However, at the locations of sharp changes in the geometry curvature, a concentration of elements was made. The elements were distributed in a sphere of radius 10^{-5}m from the vertex where the change of geometry occurs, with the minimum size of the element next to the vertex as 10^{-6}m. To achieve this concentration, triangular meshes were used instead of quadrilateral meshes. However, at the interface of the quadrilateral and triangular mesh, the meshes were joint such that each element shared a common edge. The size of the edge for both the quadrilateral mesh and the triangular mesh were the mesh parameter.

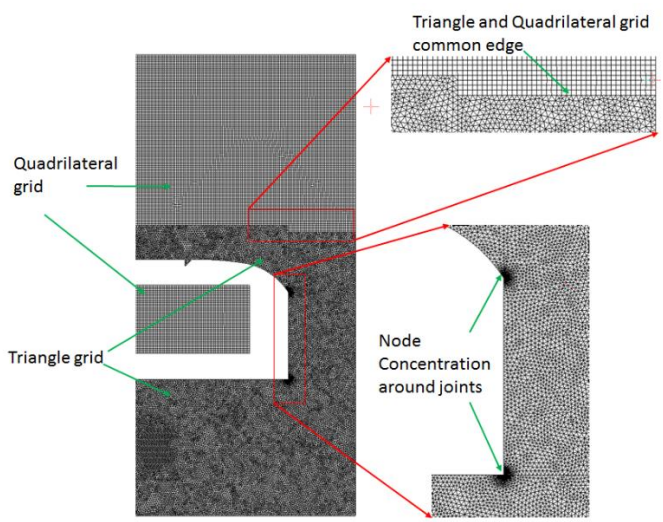

Figure 4.13 Mesh for the 2d Structural analysis showing mesh concentration near the joints.

The solver used is Ansys static structural solver, which is a finite element solver used for both linear and nonlinear static analysis. The h-method solver was used which generates a finer mesh of the already generated mesh and decreases the characteristic length of the elements to better approach the linear approximation [9].

4.6.4 Results and Discussion

At first only the pressure boundary conditions were imposed and the thermal conditions were not imposed to see the effect of just the high pressure on the probe structure. The entire domain is assumed to be at room temperature of 294K. Figure 4.14 shows the radial and axial displacement for this case along with the contours of the Von Mises stress.

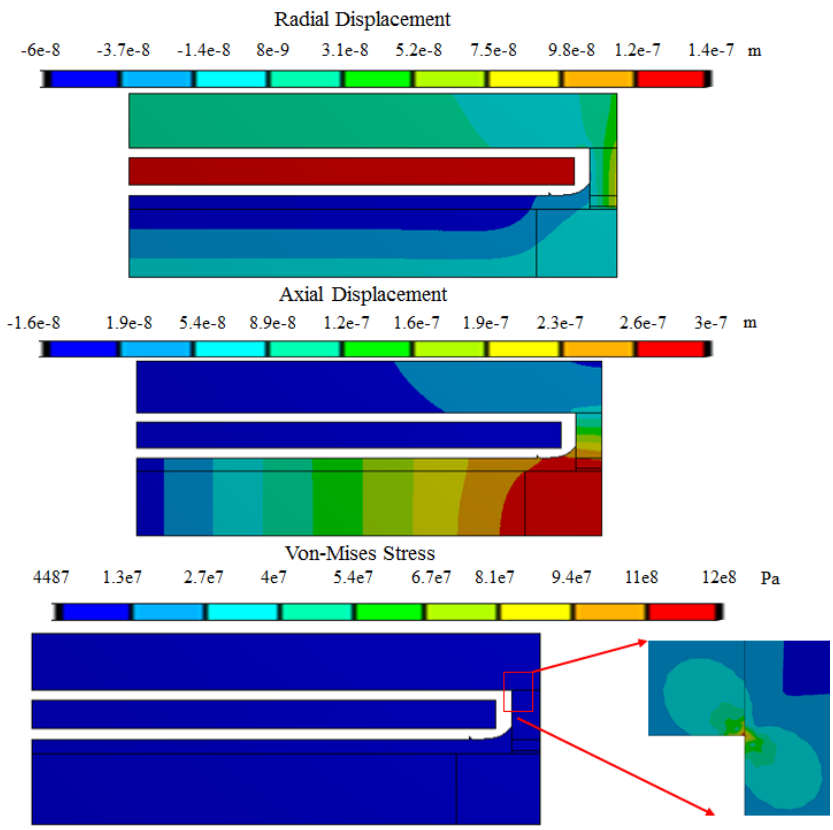

Figure 4.14 Results of the 2d structural analysis with only the pressure and shear applied, a)the radial displacement of the probe, b) the axial displacement of the probe, c) the Von-mises stress concentration of the probe.

As can be seen the effect of the pressure of the coolant does not lead to significant distortion of the structure. The maximum distortion occurs on the inner tube wall as it is deflected by the pressure difference between the inlet and outlet channel. The maximum axial displacement is obtained at the substrate due to the force exerted by the flow as its direction changes by the copper sheath and the cap of the coolant channel. However, the magnitude of both the radial and axial displacement is of the order of tenths of microns, so for all practical cases, they are negligible. The highest stress is concentrated around the sharp bends in the geometry which is an expected result. The maximum stress is still within the maximum yield strength of Inconel of $9.8X10^8$Pa. From these results, it is safe to conclude that there isn't significant impact of the very high pressure of the flow on the structural integrity of the probe and it is safe to operate it with that pressure.

When the thermal conditions discussed in 3.6.2 are included in the analysis, the contours tell a different story. All the materials expand or contract depending on the temperature, of an order of magnitude than their deformation by pressure alone as show in Figure 4.15.

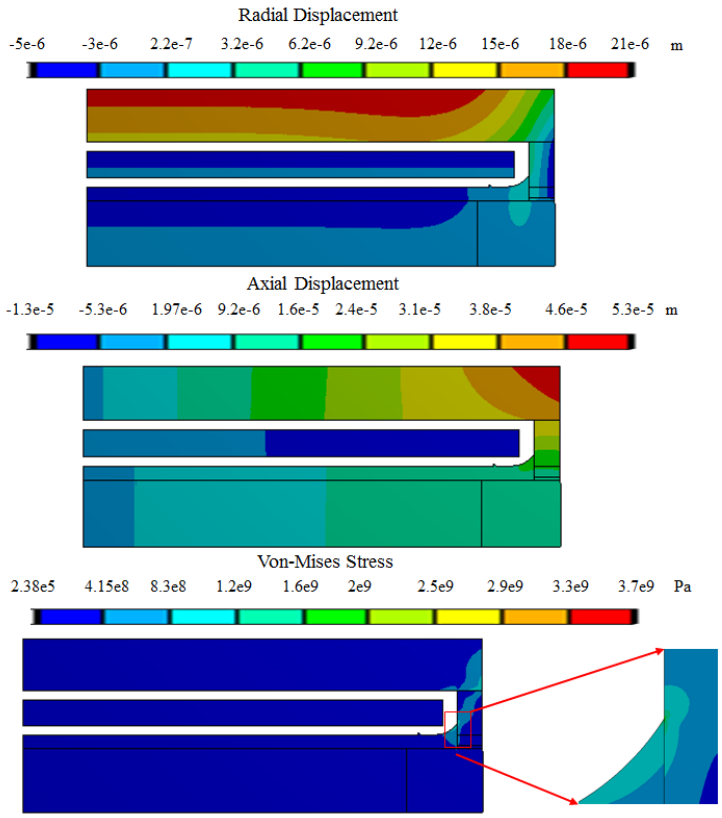

Figure 4.15 Results of the 2d structural analysis with temperature conditions applied a)the radial displacement of the probe, b) the axial displacement of the probe, c) the Von-mises stress concentration of the probe.

The greatest radial and axial displacement is seen in the outer wall of the jacket, since it is the hottest. The displacement is still of the order of microns, especially near the coolant region and does not affect the shape of the cooling channel by more than 0.5%, since the dimensions of the cooling channel are also very small. However, the sharp difference in temperature across the joints of the different materials and blocks generate tremendous stresses at those joints leading to material failure.

The limitation of this analysis is that since the thermal conditions are area averaged, across junctions of different material, the temperature gradient is high and hence there is a lot of thermally induced stress. But from the contour and by the nature of heat transfer we know that the actual gradient across these joints will not be this high, and hence the induced stress values must be much lower than that is seen in this analysis.

CHAPTER 5. CONCLUSIONS

Multiple calibration methodologies were investigated to precisely assess the uncertainty associated with the measurement of the Atomic Layer Thermopile. The aim was to obtain a linear calibration model with known uncertainty. It was found that the exposure to radiation methodology provides good linear behavior, however the uncertainty in the value of the intercept compute using the methodology from Bornstein [39], was very high. Also since there was no data regarding the surface property of the film for the wavelength of light tested, 532nm, there is high uncertainty in the actual amount of input power that was absorbed by the film that was used for calibration. Hence we see very high relative uncertainty values for low input power in the range of 2kW/m^2 computed on the uncertainty propagation model for a linear equation. The methodology of calibration against electrical power input to a heated plate exposed to flow promised lower uncertainty, however the execution of the methodology highlights several limitations chief among them being the difficulty of attaining steady state condition and attaining uniform temperature between the reference plate and the sensor film which is separated by an insulating layer of Macor. The final methodology compared the response of ALTP sensor with the heat flux calculated by wall temperature measurement for sudden discharge flow. Again good linear behavior was observed, though the calculated sensitivity was observed to be lower than that obtained with the laser exposure method, and this is attributed to a combination of uncertainty in the experiment and the drop in film sensitivity due to the hygroscopic nature of the ALTP film. The major sources of unaccounted uncertainty in this methodology were the one-dimensional assumption of heat transfer and the assumption that the heat flux at the ALTP location and wall temperature measurement location is exactly the same which assumes a perfectly two-dimensional flow field**. Through the investigation of these methodologies this work has been able to precisely obtain the uncertainty estimate that accompanies the application of the ALTP to heat flux measurement.**

The ALTP was applied to high speed flows with high frequency fluctuations by utilizing it to capture shock waves in a supersonic nozzle designed to obtain Mach 2 flow. Its response was compared to the heat flux calculated by wall temperature measurement. The ALTP shows a much higher peak in the heat flux when exposed to a shock wave consistently over several runs. It is also

able to better capture high speed fluctuations in the boundary layer when the flow transitions from supersonic to subsonic in the diverging section of the nozzle. **Thus the ALTP has been shown to be an effective sensor for supersonic environments.**

Lastly a numerical study was carried out to come up with a design for a cooling system that will allow the ALTP application in high temperature flows found inside engine combustors. The film structure limits its operational temperature to 50°C. The cooling system was designed to maintain the film at this temperature when exposed to 1000°C freestream temperature and a surrounding wall temperature of 427°C. A one-dimensional model was developed to obtain the starting parameters for a two-dimensional axisymmetric study. The one-dimensional broke the system into blocks with the average temperature of each block being the computed parameter. With the results from the one-dimensional model, a conjugate CFD analysis was carried out on a two-dimensional axisymmetric geometry. It was found that the present substrate material $SrTio_3$ was ill suited for such a cooled probe as due to its very low thermal conductivity, the substrate needs to be surrounded by -90°C isothermal wall to obtain 50°C at the film. It was decided to use an alternative substrate material of magnesium oxide which has much higher thermal conductivity. A design was found that can cool the film to 52°C. A static structural axisymmetric analysis was carried out on this geometry to ensure it can survive the high pressure necessary to pump the required amount of coolant. **With the application of this design accompanied with the precise uncertainty tools developed in this work along with the effectiveness shown of the ALTP for high speed flows, this work has demonstrated that the ALTP is a capable technique for combustor applications.**

REFERENCES

[1] Saavedra, J., Paniagua, G., Saracoglu, B., Experimental Characterization of the Vane Heat Flux Under Pulsating Trailing-Edge Blowing, ASME Journal of Turbomachinery June 2017, Vol 139 / 061004-1. doi: 10.1115/1.4035211

[2] Braun, J., Paniagua, G., Falempin, F., Naour, B., Bladeless Turbines for unsteady high speed flows, 21st AIAA International Space Planes and Hypersonics Technologies Conference, Xiamen, China, doi:10.2514/6.2017-2422

[3] Moffat, R., Describing the Uncertainties in Experimental Results, Experimental Thermal and Fluid Science 1988 0894-1777/8890043-X doi 1:3-17

[4] Lavagnoli, S., De Maesschalck, C., and Paniagua, G., Uncertainty Analysis of Adiabatic Wall Temperature Measurements in Turbine Experiments Applied Thermal Engineering, 82 pp.170-181

[5] Guo, S., Spencer, M., Lock, G., Jones, V., and Harvey, N.,1995, "The Application of Thin Film Gauges on Flexible Plastic Substrates to the Gas Turbine Situation," ASME Paper No. 95-GT-357.

[6] Thorpe, S., Yoshino, S., Ainsworth, R., and Harvey, N., 2004, "Improved Fast-Response Heat Transfer Instrumentation for Short-Duration Wind Tunnels," Meas. Sci. Technol., 15(9), pp. 1897–1909.

[7] Incropera, F., DeWitt, D., 1996 Introduction to Heat Transfer John Wiley & Sons, New York

[8] Ansys Fluent User Guide 18.1

[9] Ansys User Guide 18.1

[10] Lengfellner, H., Kremb, G., Schnellbogl, A., Betz, J., Renk, K., Prettl, W., Giant voltages upon surface heating in normal $YBa_2Cu_3O_{7-\delta}$ films suggesting an atomic layer thermopile, Applied Physics, 003-6951/92/04050-03 doi:10.1063/1.106613

[11] Cohn, J., Wolf, S., Selvamanickam, V., Salama, K., Thermoelectric power of $YBa_2Cu_3O_{7-\delta}$ phonon drag and Multiband conduction. Physical Review Letters, 66,1098 DOI:https://doi.org/10.1103/PhysRevLett.66.1098

[12] Crommie, M., Zettl, A., Barbee III, T., Cohen, M., Anisotropic thermoelectric power and conductivity in single crystal $YBa_2Cu_3O_{7-\delta}$ Physical Review Letters, 37.9734 DOI:https://doi.org/10.1103/PhysRevB.37.9734

[13] Budai, J., Chisholm, M., Feenstra, R., Lowndes, D., Norton, D., Boatner, L., Christen, D., Preferred alignment of twin boundaries in $YBa_2Cu_3O_x$ thin films and $YBa_2Cu_3O_x$ / $PrBa_2Cu_3O_x$, superlattices on $SrTiO_3$ Applied Physics Letters 003-6951/91/192174-03,doi:10.1063/1.104997

[14] Capponi, J., Chaillout, C., Hewat, A., Lejay, P., Marezio, M., Nguyen, N., Raveau, B., Soubeyroux, J., Tholence, J., Tournie, R., Structure of the 100 K Superconductor Ba2YCu307 between (5 + 300) K by Neutron Powder Diffraction. Europhys. Lett., 3 (12)) pp. 1301-1307 (1987) doi 10.1209/0295-5075/3/12/009

[15] Brent, H., Crystal Structure and Superconductivity of $YBa_2Cu_3O_{7-\delta}$ Thesis submitted to Minnesota State University, Mankato, Minnesota July 2014

[16] Roediger, T., Knauss, H., Gasibauer, U., Kraemer, E., Jenkins, S., Wolfersdorf, J., Time Resolved Heat Transfer Measurements on the Tip Wall of a Ribbed Channel Using a Novel Heat Flux Sensor—Part I: Sensor and Benchmarks Journal of Turbomachinery January 2008, Vol. 130 / 011018-1 doi 0.1115/1.2751141

[17] Zhang, P., Lee, W., Zhang, G., Time dependence of laser-induced thermoelectric voltage in $La_{1-x}Ca_xMnO_3$ and $YBa_2Cu_3O_{7-\delta}$ thin films Applied Physics Letter 0003-6951/2002/81(21)/4026/3/ doi 10.1063/1.1520712

[18] Carslaw, H., and Jeager, J., Conduction of Heat in Solids, Oxford at the Clarendon Press

[19] Knauss, H., Gasibauer, U., Wagner, S., Buntin, D., Maslov, A., Smorodsky, B., Betz, J., Calibration experiments of a new active Fast response heat flux sensor to measure Total temperature fluctuations Part 1. Introduction to the problem ICMAR-2002 International Conference on the Methods of Aerophysical Research: Proc. Pt I–III, Novosibirsk.

[20] Roediger, T., Knauss, H., Wagner, S., Kraemer, E., Bountin, D., Smorodsky, B., Chirkashenko, V., Zvegintsev, V., Maslov, A., The Atomic Layer Thermopile - a fast heat flux sensor for measuring high heat loads in short duration Hypersonic Ground Testing facilities ICMAR 2007

[21] Lejsek, D., Kulzer, A., Investigations on the Transient Wall Heat Transfer at Start-Up for SI Engines with Gasoline Direct Injection, SAE International Journal of Engines Vol2 no1 2009 pp. 381-397 Stable URL: https://www.jstor.org/stable/26308405

[22] Kegerise, M., Rufer, S., Unsteady Heat-Flux Measurements of Second-Mode Instability Waves in a hypersonic flat plate boundary layer, S.J. Exp Fluids (2016) 57: 130.doi /10.1007/s00348-016-2214-9

[23] Holmberg, D., Steckler, K., Womeldorf, C., Grosshandler, W., Facility for Calibrating Heat Flux Sensors in a Convective Environment, Proceedings of the ASME Heat Transfer Division HTD-Vol353 Volume 3 ASME 1997 165–71

[24] Holmberg, D., Womenldorf, C., Grosshandler, W., Design and Uncertainty Analysis of a second generation convective heat flux calibration facility HTD Vol-364-4 Proceedings of the ASME Heat Transfer Division – 1999 Volume 4 ASME 1999 65-70

[25] Borell, G., Diller, T., A Convection Calibration Method for local Heat Flux Gauges, Journal of Heat Transfer February 1987 Vol 109/83 doi:10.1115/1.3248073

[26] Pullins, C., Diller, T., In situ high temperature heat flux sensor calibration, International Journal of Heat and Mass Transfer 53(17-18) (2010)3429-3438

[27] Jenkins, S., von Wolfersdorf, J., Weigand, B., Roediger, T., Knauss, H., Kraemer, E., Time Resolved Heat Transfer Measurements on the Tip Wall of a Ribbed Channel using a Novel Heat Flux Sensor – Part – II Heat Transfer Results, Journal of turbomachinery January 2008 Vol 130/011019-1 doi:10.1115/1.2472417

[28] Meyer, R., 1960, "A Heat Flux Meter for Use with Thin Film Surface Thermometers," NRC Canada, Aero. Rep. LR-279.

[29] Oldfield, M., Burd, H., and Doe, N., 1982, "Design of Wide Bandwidth Analogue Circuits for Heat Transfer Instrumentation in Transient Tunnels," 16th Symp. of 1CHMT, Dubrovnik, Hemisphere Publ., Washington, DC.

[30] Doorly, J., 1988, "Procedures for Determining Surface Heat Flux Using Thin Film Gages on a Coated Metal Model in a Transient Test Facility," ASME Journal of Turbomachinery, Vol. 110, Pp. 242-250

[31] Ainsworth, R., Allen, J., Davies, M., Doorly, J., Forth, C., Hilditch, M., Oldfield, M., Sheard, A., Developments in Instrumentation and Processing for Transient Heat Transfer Measurement in a Full-Stage Model Turbine, ASME Journal of Turbomachinery 111(1), 20-27 (Jan 01, 1989) (8 pages) doi:10.1115/1.3262232

[32] Van Treuren, K., Wang, Z., Ireland, P., Jones, T., Detailed Measurements of Local Heat Transfer Coefficient and Adiabatic Wall Temperature beneath an array of impinging jets. ASME Journal of Turbomachinery 116(3), 369-374 (Jul 01, 1994) doi:10.1115/1.2929423

[33] Gritsch, M., Schulz, A., Wittig, S., Adiabatic Wall Effectiveness Measurements of Film-Cooling Holes with Expanded Exits Paper No. 97-GT-164, pp. V003T09A029 doi:10.1115/97-GT-164

[34] Hanby, V., Convective Heat Transfer in a Gas-Fired Pulsating Combustor ASME *J. Eng. Power* 91(1), 48-52 (Jan 01, 1969) (5 pages) doi:10.1115/1.3574675

[35] Watanabe, H., Harada, T., Hoshino, K., Matsushita, Y., Aoki, H., Miura, T., An Experimental Investigation of the Characteristics of the Secondary Atomization and Spray Combustion of Emulsified Fuel, Journal of Chemical Engineering of Japan, doi-10.1252/jcej.08we144

[36] Marshall, W., Pal, S., Wodward, R., Santoro, R., Benchmark Wall Heat Flux Data for a GO_2/GH_2 Single Element Combustor 41st AIAA/ASME/SAE/ASEE Joint Propulsion Conference & Exhibit AIAA Paper 2005-3572, 2005

[37] Ireland, P., Jones, T., Liquid crystal measurements of heat transfer and surface shear stress 2000 Measurement Science and Technology doi-10.1088/0957-0233/11/7/313

[38] Celik, I., Ghia, U., Roache, P., Freitas, C., Coleman, H., Raad, P., Procedure for Estimation and Reporting of Uncertainty Due to Discretization in CFD Applications ASME Journal of Fluids Engineering 130(7), 078001 (Jul 22, 2008) (4 pages) doi:10.1115/1.2960953

[39] Bornstein, I., and Semendjajew, K., Tuschenbuch der Marhemafik. Harry Deutsch. Thun (1980).

[40] Lin, J., West, J., Williams, R., Tucker, P., and Chenoweth, J., "CFD Code Validation of Wall Heat Fluxes for a GO2=GH2 Single Element Combustor," 41st AIAA/ASME/SAE/ASEE Joint Propulsion Conference and Exhibit, AIAA Paper 2005-4524, July 2005.

[41] Cook, W., and Felderman, E., "Reduction of data from thin-film heat-transfer gages - A concise numerical technique." AIAA Journal, Vol. 4, No. 3 (1966), pp. 561-562 doi 10.2514/3.3486

[42] Menezes, V., Bhat, S., A coaxial thermocouple for shock tunnel applications Review of Scientific Instruments 81, 104905 (2010); https://doi.org/10.1063/1.3494605

[43] Owen, F., Transition experiments on a flat plate at subsonic and supersonic speeds", AIAA Journal, Vol. 8, No. 3 (1970), pp. 518-523 doi: 10.2514/3.5699

[44] Beresh, S., Henfling, J., Spillers, R., Preutt, B., Fluctuating wall pressures measured beneath a supersonic turbulent boundary layer, Physics of Fluids 23, 075110 (2011); doi: 10.1063/1.3609271